Sociosexual behavior requires both activating and repressive roles of Tfap2e/AP-2ε in vomeronasal sensory neurons

Jennifer M. Lin[1,2†], Tyler A. Mitchell[1,2†], Megan Rothstein[3], Alison Pehl[1,2], Ed Zandro M. Taroc[1,2], Raghu Ram Katreddi[1,2], Katherine E. Parra[4], Damian G. Zuloaga[4], Marcos Simoes-Costa[3], and Paolo E. Forni[1,2,*]

[1]Department of Biological Sciences, University at Albany, Albany, NY, USA.

[2]The RNA Institute, University at Albany, Albany, NY, USA.

[3]Department of Molecular Biology and Genetics, Cornell University, Ithaca, New York 14850, USA

[4]Department of Psychology, University at Albany, Albany, NY, USA.

[†]Authors contributed equally

*Corresponding Author

SUMMARY

Neuronal identity dictates the position in an epithelium, and the ability to detect, process, and transmit specific signals to specified targets. Transcription factors (TFs) determine cellular identity via direct modulation of genetic transcription and recruiting chromatin modifiers. However, our understanding of the mechanisms that define neuronal identity and their magnitude remains a critical barrier to elucidate the etiology of congenital and neurodegenerative disorders. The rodent vomeronasal organ provides a unique system to examine in detail the molecular mechanisms underlying the differentiation and maturation of chemosensory neurons. Here we demonstrated that the identity of postmitotic/maturing vomeronasal sensory neurons (VSNs), and vomeronasal dependent behaviors can be reprogrammed through the rescue of tfap2e/AP-2ε expression in the AP-2ε^{Null} mice, and partially reprogrammed by inducing ectopic AP-2ε expression in mature apical VSNs. We suggest that the transcription factor AP-2ε can reprogram VSNs bypassing cellular plasticity restrictions, and that it directly controls the expression of batteries of vomeronasal genes.

KEYWORDS

Vomeronasal, Transcription Factor, Tfap2e/AP-2ε, Neuronal Identity, Single-Cell Sequencing, scRNA-seq, CUT&RUN, Chromatin Architecture, Cellular Plasticity, behavior, basal vomeronasal sensory neurons, accessory olfactory bulb, differentiation

INTRODUCTION

Neuronal differentiation is controlled by the selective expression of transcription factors (TFs), chromatin modifiers, and other regulatory factors that reduce cellular plasticity. During neuronal differentiation terminal selectors can activate identity-specific genes that define functional properties specific to a particular neuronal type. However, reprograming postmitotic neurons by ectopically expressing terminal selectors in *C. elegans* suggests that the "reprogrammability" of neurons is progressively lost during postembryonic life (Patel and Hobert, 2017; Patel et al., 2012; Rahe and Hobert, 2019). This reduction in cellular plasticity may arise from chromatin modifications that prevent the activation of alternative differentiation programs. However, sensory neurons of the vomeronasal organ in rodents can undergo some postnatal reprogramming following the aberrant expression of transcription factors (Lin et al., 2018).

The accessory olfactory system (AOS) contains the vomeronasal organ (VNO), which is primarily responsible for detecting odors and chemosignals that trigger social and sexual behaviors (Trouillet et al., 2019; Trouillet et al., 2021). The vomeronasal sensory epithelium of rodents is mainly composed of vomeronasal sensory neurons (VSNs). The VSN populations selectively express only one or two receptors encoded by the two vomeronasal receptor (VR) gene families: V1R and V2R (Dulac and Axel, 1995; Herrada and Dulac, 1997; Matsunami and Buck, 1997; Ryba and Tirindelli, 1997). V1R and V2R-expressing neuronal populations each detect distinct chemosignals, induce different innate behaviors, show distinct localization patterns in the VNO, and project to specific areas of the accessory olfactory bulb (AOB) (Cloutier et al., 2002; Dulac and Axel, 1995; Isogai et al., 2011; Katreddi and Forni, 2021; Mohrhardt et al., 2018; Mombaerts et al., 1996; Stowers et al., 2002). The V2R-expressing neurons localize to the basal portions of the vomeronasal epithelium (VNE) and around the vasculature (Naik et al.,

2020), while V1R-expressing neurons localize to the apical part. Basal and apical VSNs continually regenerate from common pools of Achaete Scute like-1 (Ascl-1)-positive neural progenitor cells (NPCs) localized in the lateral and basal margins of the VNE (Cau et al., 1997; de la Rosa-Prieto et al., 2010; Katreddi and Forni, 2021; Martinez-Marcos et al., 2000; Murray et al., 2003). However, we are only starting to understand how the apical and basal VSN cell differentiation programs are initiated and which factors aide in maintaining apical and basal neuronal identity (Enomoto et al., 2011; Katreddi et al., 2022; Lin et al., 2018; Naik et al., 2020; Oboti et al., 2015).

Establishing functional basal and apical VSNs is crucial for intra- and interspecies social interactions in rodents. Deficits in basal neuron functionality prevented sex discrimination, reduced male-male and maternal aggressive behaviors, and inhibited the detection of predator odors (Chamero et al., 2011; Stowers et al., 2002).

Transcription factors can drive cellular processes that control the expression of genes defining their cellular and functional identity. The AP-2 family of transcription factors is comprised of 5 members AP-2α, AP-2β, AP-2γ, AP-2δ and AP-2ε, which are encoded by distinct genes (TFAP2A, TFAP2B, TFAP2C, TFAP2D, TFAP2E) (Eckert et al., 2005; Pellikainen and Kosma, 2007; Wankhade et al., 2000). AP-2 family members play critical roles during development, such as contributing to neural crest differentiation (Luo et al., 2020; Rothstein and Simoes-Costa, 2020), cell specification, limb development, and organogenesis (Bassett et al., 2012; Chambers et al., 2019; Kantarci et al., 2015). Some AP-2 family members may have pioneer factor properties (Fernandez Garcia et al., 2019; Rothstein and Simoes-Costa, 2020; Seberg et al., 2017; Williams et al., 2009).

Aside from AP-2ε , Notch signaling and Bcl11b control Gαo+ VSNs' differentiation, homeostasis, and survival (Enomoto et al., 2011; Katreddi et al., 2022). We previously proposed that AP-2ε, which is only expressed after the apical and basal VSN dichotomy is established, is necessary for further specification of basal VSN identity (Lin et al., 2018). Using mice expressing non-functional AP-2ε, we discovered that VSNs can still acquire the Gαo+/basal identity; however, these VSN have reduced survival and can acquire some Gαi2+/apical VSNs molecular features over time (Lin et al., 2018). While we examined the role of AP-2ε in maintaining cellular identity and homeostasis of the

95 vomeronasal epithelium, critical outstanding questions remain unresolved. What role
96 does this transcription factor actively play to control the basal genetic program? What is
97 the extent of cellular plasticity in differentiated neurons in mammals (Patel and Hobert,
98 2017; Rahe and Hobert, 2019)?

99 Here, we aimed to understand 1) if AP-2ε functions as a terminal selector factor
100 for basal VSNs, 2) how much cellular plasticity postmitotic neurons retain once
101 differentiated, and 3) to what extent genetic dysregulation in mature VSNs translates into
102 behavioral changes. We generated a Cre inducible mouse line, where we inserted the
103 mTfap2e/AP-2ε gene into the ROSA26 locus. Using this knock-in mouse line, we could
104 1) rescue the AP-2ε KO's VNO morphology and functionality and 2) ectopically express
105 AP-2ε in maturing Gαi2+/apical VSNs. This approached enable us to assess its ability to
106 reprogram differentiated apical VSNs to basal VSNs. By combining histological analyses,
107 behavioral assessments, and single-cell RNA sequencing (scRNA-seq) analysis, we
108 examined whether AP-2ε functions as a master regulator to reprogram differentiated
109 neurons and alter animal behaviors. In addition, we used CUT&RUN (Skene et al., 2018)
110 to identify direct genetic targets of AP-2ε that controls the basal VSNs identity program.
111 Overall, we suggest that AP-2ε partially functions as a terminal selector by activating
112 some basally enriched genes while simultaneously suppressing specific apically enriched
113 genes.
114
115
116 **RESULTS**
117 **Transcriptome differences between apical and basal VSNs**
118 Using single cell RNA-sequencing (scRNA-Seq) on VNOs from OMPCre+ control
119 mice at P10, we identified key features of VSNs based on the expression plots. We then
120 clustered single cells into representative Uniform Manifold Approximation and Projections
121 (UMAPs) (Figure 1). Achaete-Scute Family BHLH Transcription Factor 1 (Ascl1), (Figure
122 1A), Neurogenin1 (Neurog1) (Figure 1B), and NeuroD1 (Figure 1C) expression identified
123 proliferative VSN progenitors (Katreddi and Forni, 2021). We determined that the
124 dichotomy of apical-basal differentiation begins when the cells transition from Neurog1 to
125 NeuroD1 expression, and during the NeuroD1 phase (Figure 1B,C)(Katreddi et al., 2022).

126 The later stages of apical and basal VSN maturation were marked by the expression of
127 Gap43 (Figure 1D) in immature VSNs and OMP (Figure 1E) in more mature VSNs
128 (Katreddi and Forni, 2021).
129 Consistent with prior reports, the mRNA for the transcription factor Bcl11b (Figure
130 1F) was found to be expressed in Neurog1+/NeuroD1+ (Figure 1B,C) precursors and in
131 differentiating apical and basal VSNs. While Bcl11b was expressed as a continuum along
132 the basal differentiation trajectory, in the apical neurons, Bcl11b was not expressed until
133 later stages of maturation (Figure 1F) (Enomoto et al., 2011; Katreddi et al., 2022). The
134 transcription factor Meis2 was expressed in progenitor cells as well as in apical VSNs'
135 differentiating neurons (Figure 1G). These also express Gnai2/ Gαi2, Nrp2 and V1rs at
136 more mature stages (Figure 1I-K). On the other side, mRNA for the transcription factors
137 Tfap2e/AP-2ε (Figure 1K) was found to be expressed, in line with our prior works
138 (Katreddi et al., 2022; Lin et al., 2018), in differentiating/maturing and mature basal VSNs.
139 The basal VSNs' differentiation trajectory was further confirmed by the expression of
140 known V2r/basal VSNs' markers such as Robo2, Gnao1/Gαo, and Vnm2r receptors
141 (Figure 1K-N). In addition, our transcriptome analysis revealed significant enrichments
142 ($q<0.05$, Figure 1Q, Supplementary Table S1) of several previously unreported genes in
143 either apical or basal VSNs. Fbxo17, Mt3 (Figures 1O,P; S5) and Keratin18 (Krt18), were
144 among the genes that we found enriched in maturing basal VSNs.
145
146 **Inducible R26AP2ε rescues basal VSNs in AP-2ε KOs**
147 We hypothesized that Tfap2e (AP-2ε) can control gene expression during basal
148 VSN maturation. So, we generated a new Cre inducible mouse line (B6.Cg-
149 Gt(ROSA)26Sor$^{tm(CAG\text{-}mTfap2e)For}$). We inserted a lox-P-flanked stop cassette to prevent the
150 transcription of a CAG promoter driven murine Tfap2e gene, which was knocked into the
151 first intron of the Gt(ROSA)26Sor locus (Figure 2A). We refer to this as R26AP2ε. AP-2ε
152 expression is normally restricted to basal regions of the VNO with higher expression
153 levels of AP-2ε in the neurogenic marginal zones (Enomoto et al., 2011; Lin et al., 2018;
154 Naik et al., 2020)(Figures 1; 2B,B'). To test our Cre inducible AP-2ε line, we performed
155 anti-AP-2ε immunostaining on wild-type controls, AP-2ε$^{Cre/Cre}$ (AP-2ε^{Null})(Feng et al.,
156 2009; Lin et al., 2018), and AP-2ε$^{Cre/Cre}$/R26AP2ε (AP-2ε^{Rescue}) mice (Figure 2B-D). As

157 expected, (Lin et al., 2018), wild-type mice showed AP-2ε immunoreactivity in the basal
158 regions of the VNE with strong immunoreactivity in the neurogenic regions (Figure 2B,
159 B'). However, in AP-2ε^{Null} mice, where Cre was knocked into the DNA binding domain of
160 AP-2ε (Feng et al., 2009; Feng and Williams, 2003), we observed faint AP-2ε cytoplasmic
161 immunoreactivity limited to the most marginal zones of the VNO and no immunoreactivity
162 in the rest of the neuroepithelium (Figure 2C,C'). AP-2ε^{Rescue} mice showed restored AP-
163 2ε immunoreactivity in the basal region of the VNE (Figure 2D). However, we observed
164 that the AP-2ε expression pattern and immunoreactivity were not identical to controls in
165 the neurogenic regions. In AP-2ε^{Rescue} mice, we observed no AP-2ε immunoreactivity at
166 the tips of the neurogenic niche in the VNE (Figure 2D'), suggesting a delayed AP-2ε
167 expression after AP-2εCre mediated recombination compared to controls (Figure 2B',D').
168 By analyzing the expression of the basal markers downregulated in AP-2ε KOs
169 (Lin et al., 2018), such as V2R2 (Figure 2E-G) and Gαo (Figure 2H-J), we confirmed
170 restored expression in the rescued KOs. Cell quantifications indicated a significant
171 increase in the number of basal cells expressing basal markers in AP-2ε^{Rescue} compared
172 to AP-2ε^{Null} mice, though the number of basal VSNs in the AP-2ε^{Rescue} was smaller when
173 compared to controls (Figure 2N). Keratin18 (Krt18) is normally enriched in basal neurons
174 (Figure 1Q). Immunohistochemistry confirmed Krt18 protein expression in the basal
175 territories of the VNO (Figure 2K). We observed reduced Krt18 immunoreactivity in AP-
176 2ε^{Null} mice and restored expression in AP-2ε^{Rescue} mice (Figure 2L-N). However, in AP-
177 2ε^{Rescue} mice, Krt18 still showed lower expression levels than in WT mice (Figure 2N).
178 Taken together, we conclude that exogenous AP-2ε in postmitotic VSNs can partially
179 rescue the expression of basal VSN markers in AP-2ε^{Nulls} mice. Rescue of the AP-2ε^{null}
180 phenotype indicates that our inducible R26AP2ε mouse line is a suitable model for
181 conditional expression of functional AP-2ε.
182
183 **Re-expressing AP-2ε in AP-2ε mice rescues social behaviors**
184 The specification and organization of VSNs and their respective circuit assembly
185 in the AOB are essential to trigger a variety of social and sexual behaviors (Chamero et
186 al., 2011; Chamero et al., 2007; Stowers et al., 2002; Trouillet et al., 2019) . We

187 speculated that AP-2ε^{Null} mice could not discriminate between urine of different sexes.
188 Thus, we performed an odorant preference test. In this test, individual mice were
189 simultaneously presented with male and female whole urine for a two-minute period
190 (Figure 3A). Wild-type male mice showed a significant preference for urine from the
191 opposite sex (Figure 3B)(Pankevich et al., 2004; Stowers et al., 2002). However, AP-2ε^{Null}
192 male mice did not display significant preference for female urine, confirming a loss of
193 function (LOF) of basal VSNs (Lin et al., 2018) and consequently a reduced ability to
194 discriminate between urine from either sex (Figure 3B)(Pankevich et al., 2004; Stowers
195 et al., 2002). However, AP-2ε^{Rescue} male mice showed a significant preference for female
196 urine similar to WT controls (Figure 3B).

197 To further investigate the behavioral outcome of AP-2ε LOF and AP-2ε re-
198 expression in AP-2ε^{Null} mice, we performed a resident intruder assay for intermale
199 aggression (Figure 3C)(Chamero et al., 2011; Montani et al., 2013; Stowers et al., 2002).
200 Wild-type male mice showed aggressive behaviors toward intruders upon detecting male
201 specific odorants (Figure 3D). Most AP-2ε^{Null} mice did not attack the intruder (Figure 3D).
202 Yet, when male AP2$\varepsilon^{Cre/Cre}$/R26AP2$\varepsilon^{+/-}$ (AP-2ε^{Rescue}) mice were exposed to male
203 intruders, they displayed aggressive behavior similar to that of controls (Figure 3D). We
204 measured the mass of the seminal vesicles from each genotype to rule out any changes
205 in general androgen levels, which may explain any potential behavioral differences
206 (Zuloaga et al., 2007). We found no significant differences when the seminal vesicle
207 weights were normalized to the total body weight of each mouse (Figure 3E). Taken
208 together, these data suggest re-expression of AP-2ε in KO mice can reestablish the
209 functional properties of basal VSNs.
210

211 **Ectopic expression of AP-2ε in mature apical VSNs increases the expression of**
212 **basal enriched genes**

213 Several AP-2 family members have been proposed to have pioneer activity
214 (Fernandez Garcia et al., 2019; Rothstein and Simoes-Costa, 2020; Seberg et al., 2017;
215 Williams et al., 2009). We tested whether ectopic AP-2ε expression can alter the
216 transcriptomic profile of maturing neurons. Olfactory marker protein (OMP) is an accepted

217 marker for postmitotic/maturing olfactory and vomeronasal sensory neurons (Buiakova et
218 al., 1994; Enomoto et al., 2011; Farbman and Margolis, 1980). By analyzing our scSeq
219 data from OMPCre$^{+/-}$ mice, we confirmed that OMP mRNA expression can be detected in
220 maturing apical neurons shortly after the apical basal dichotomy is established (Figure
221 1E). Thus, we used an OMPCre mouse line to drive expression of AP-2ε (OMPCre$^{+/-}$
222 /R26AP2ε$^{+/-}$) in all olfactory and vomeronasal neurons. In this manuscript we will often
223 refer to OMPCre$^{+/-}$/R26AP2ε$^{+/-}$ as ectopic mutants. Notably, both apical and basal VSNs
224 express several known Tfap2 cofactors, including Cited2 and p300/CBP (Bamforth et al.,
225 2001; Bragança et al., 2003; Eckert et al., 2005) suggesting that both VSN populations
226 are molecularly competent for functional AP-2ε transcriptional activity (Figure S1).

227 Immunostaining against AP-2ε showed no immunoreactivity in the main olfactory
228 epithelium (OE) of control animals (Figure S2A). However, in OMPCre$^{+/-}$/R26AP2ε$^{+/-}$
229 mutants, the OE expressed immunodetectable AP-2ε (Figure S2C). OMPCre$^{+/-}$ controls
230 and OMPCre$^{+/-}$/R26AP-2ε$^{+/-}$ mutants displayed comparable gross morphology of the OE
231 with no ectopic V2R immunoreactivity (Figure S2B,D).

232 In the VNO of OMPCre$^{+/-}$ controls, AP-2ε was found only in cells in the basal
233 territory (Figure 4A, A1). However, in OMPCre$^{+/-}$/R26A-P2ε$^{+/-}$ mice, we found that virtually
234 all the VSNs expressed AP-2ε (Figure 4D, D1). In these mutants we also observed AP-
235 2ε expression in sparse sustentacular cells lining the lumen of the VNO (Figure 4D).

236 When comparing the VNO of P10 controls (either WT or OMPCre$^{+/-}$) and
237 OMPCre$^{+/-}$/R26AP-2ε$^{+/-}$ mutants, we observed that the ectopic mutants had a significantly
238 broader Gαo mRNA expression across the VNE (Figure 4B,E). As the broader expression
239 was hardly conducible to individual cells we performed a densitometric analysis of
240 sections after *in-situ* hybridization (ISH). This indicated that, in the mutants, a larger
241 percentage of the VNE was positive for Gαo expression (Figure 4G). Moreover, we found
242 that OMPCre$^{+/-}$/R26AP2ε$^{+/-}$ mutants had a larger number of cells immunodetectable using
243 the anti V2R2 antibody (Silvotti et al., 2011) (Figure 4C,F,H). These immunoreactive cells
244 could be found spanning from basal VNO regions to the lumen.

245 In line with these observations scRNA-Seq data from OMPCre$^{+/-}$ controls and
246 OMPCre$^{+/-}$/R26AP2ε$^{+/-}$ indicated that apical VSNs expressing AP-2ε had variable, but

247 significant (P<0.05) upregulation, of Gαo mRNA as well as increased expression for
248 some C family Vmn2r, many of which can be detected using the anti V2R2 antibody
249 (Figures 4I,J; S2E-H) (Silvotti et al., 2011). Notably our scRNA-Seq data indicated that
250 that low/basal levels of Vmn2r7 mRNA expression can be also detected in sparse apical
251 neurons of controls (Figures 4I; S2E-H).

252 Immunostaining against V2R2 and Meis2 also highlighted that, while in controls,
253 Meis2 and V2R2 remained segregated (Figure 4K), in the ectopic mutants, V2R receptors
254 could be immunodetected in Meis2+ apical neurons (Figure 4L). These data suggest that
255 ectopic AP-2ε expression can induce or increase the expression of basal enriched genes.

256 In order to better follow the effects of ectopic AP-2ε expression on apical cells we
257 also performed RNAscope analysis using probes against the basal VSN marker Gαo and
258 the apical markers Gαi2 and Meis2 (Figure 4M,N).

259 In controls (Figure 4M), we could observe a clear segregation between the basal
260 VSNs positive for Gαo and the apical VSNs positive for Meis2 and Gαi2. Notably Meis2
261 was also expressed in the sustentacular cells and in newly formed cells in the marginal
262 zone. However, in OMPCre$^{+/-}$/R26AP2ε$^{+/-}$ mutants (Figure 4N), we could observe, as after
263 regular ISH (Figure 4E) a low but obvious expansion of Gαo expression to the apical
264 domains of the VNO. Signal highlighting Gαo expression could be found in Meis2 and
265 Gαi2 positive cells.

266

267 **Ectopic AP-2ε expression leads to a progressive disorganization of the VNE**

268 In ectopic AP-2ε mutants at P21, and more dramatically at 3 months of age, we
269 noticed an increasing level of cellular disorganization of the VNE not seen in controls
270 (Figure 5A,A') with: 1) VSNs spanning from the basal territories to regions of the lumen
271 devoid of Sox2+ sustentacular cells, and 2) ectopic sustentacular cells organized in
272 spherical structures or intraepithelial cysts with a subsidiary lumen within apical and basal
273 territories (Figure 5B-C'). Notably, the regions with ectopic sustentacular cells appeared
274 to be mostly surrounded by apical VSNs expressing AP-2ε, Meis2, and Sox2 and were
275 enriched in the intermediate zones of the VNE (Figure 5B-D). Interestingly, a low level of
276 Sox2 immunoreactivity was observed in apical VSNs in both controls and OMPCre$^{+/-}$

277 /R26AP2$\varepsilon^{+/-}$ mice with higher intensity in cells closer to the sustentacular cell layer (Figure
278 S3A,B,D,E).
279 The affinity and positioning of epithelial cells are largely dictated by the expression
280 of surface adhesion molecules (Fagotto, 2014; Polanco et al., 2021). Transcriptome
281 comparison of OMPCre$^{+/-}$/R26AP2$\varepsilon^{+/-}$ mutants and controls suggest that the aberrant cell
282 positioning in the VNE of mutants can arise from broad variations in expression levels of
283 multiple adhesion molecules throughout Meis2+ cells (Figure 5E).
284 Furthermore, scRNA-Seq of the adult OMPCre$^{+/-}$/R26AP2$\varepsilon^{+/-}$ allowed us to
285 understand whether sustentacular cells with ectopic AP-2ε expression was contributing
286 to the disorganization of the VNE. By performing differential gene expression analysis on
287 the AP-2ε positive and negative sustentacular cells from the adult OMPCre$^{+/-}$/R26AP2$\varepsilon^{+/-}$
288 mice we observed significantly dysregulated genes (550 upregulated; 571
289 downregulated, adjusted p-value<0.05) with enrichment of genes related to tight-
290 junctions, cell-cell adhesion, and cytoskeletal organization (Figure S3G-I), which may
291 contribute to the disorganized neuroepithelium.
292
293 **Ectopic expression of AP-2ε alters the transcriptional profile of apical neurons**
294 To further elucidate the gene expression changes in apical (Meis2+) VSNs after
295 AP-2ε expression, we analyzed the UMAPs using scSeq from VSNs in controls and
296 mutant mice. These revealed similar clustering at the stages of neurogenesis and
297 differentiation across genotypes (Figure 7A-B). However, control animals showed AP-2ε
298 expression was limited to immature-mature basal VSNs (Figures 7A'-A'''; 4A1). In
299 OMPCre$^{+/-}$/R26AP-2$\varepsilon^{+/-}$ mutants, however, AP-2ε mRNA was expressed in maturing
300 basal VSNs as well as in maturing and mature apical VSNs (Figures 7B', B'''; 4D1). When
301 analyzing the UMAPs, we noticed that in the OMPCre$^{+/-}$/R26AP-2$\varepsilon^{+/-}$ mutants, cells along
302 the apical and basal developmental trajectories overlapped to those of controls. However,
303 the maturing and mature apical VSNs of controls and mutants formed non overlapping
304 clusters (Figure 7A'''-(A+B)''''). In fact, the apical VSNs of the ectopic mutants formed a
305 cluster more proximal to the basal VSNs.

306 To understand the extent to which AP-2ε can reprogram apical VSNs, we further
307 compared the expression of the most enriched genes in apical and basal VSNs of
308 OMPCre$^{+/-}$ controls to the apical VSNs of OMPCre$^{+/-}$/R26AP-2ε$^{+/-}$. Interestingly, this
309 analysis revealed that apical VSNs of OMPCre$^{+/-}$/R26AP-2ε$^{+/-}$ mice had a mixed apical-
310 basal RNA expression profile with a significant down-regulation of ~22% of the apical-
311 enriched genes (7/32), and a significant upregulation of ~28% of the basal-enriched
312 genes (20/71) (Figure 7C; Supplementary Table S2). Performing a correlation analysis,
313 we observed that while in controls, sets of either apical or basal enriched genes had
314 high correlation, this was no longer true for the OMPCre$^{+/-}$/R26AP-2ε$^{+/-}$ mutants (Figure
315 S4).
316 Of the aberrantly expressed genes in the apical VSNs of OMPCre$^{+/-}$/R26AP-2ε$^{+/-}$
317 mice, we identified a reduction in Calreticulin (Calr) mRNA levels together with a strong
318 upregulation of Calreticulin4 (Calr4), which persists in adulthood (Figure 7D-G,
319 Supplementary Table S2, Figure S8A,C). Calr is a negative regulator of transport of V2R
320 receptors to the cell membrane (Dey and Matsunami, 2011). ISH at P11 confirmed that
321 Calr4 is normally expressed by basal VSNs in controls. However, in OMPCre$^{+/-}$
322 /R26AP2ε$^{+/-}$ mutants, Calr4 mRNA was found in both apical and basal VSNs (Figure
323 7F,G). In line with previous studies (Dey and Matsunami, 2011), we found that Calr was
324 expressed below ISH detectability. Feature maps also pointed to the ectopic expression
325 in apical VSNs of other basal enriched genes such as Gαo (Figures 4; S5A), Mt3, and
326 Fbxo17 (Figure S5B,D). In apical cells these genes are normally either silenced in mature
327 VSNs or absent from the beginning of the differentiation. RNAscope analysis for Mt3
328 confirmed ectopic expression in apical cells (Figure S5C).
329
330 **OMPCre$^{+/-}$/R26AP-2ε$^{+/-}$ ectopic mutants have normal axonal projections to the AOB**
331 Axonal projection along the anterior posterior axis of the AOB is largely determined
332 by axon guidance molecules such as Nrp2, Robo2 while the the coalescence of
333 vomeronasal sensory neuron axons into glomeruli is largely dictated by Kirrel adhesion
334 molecules (Cloutier et al., 2002; Prince et al., 2013; Prince et al., 2009; Vaddadi et al.,
335 2019). The mRNA expression levels for the guidance receptors, Robo2 and Nrp2, and
336 the adhesion molecules, Kirrel2 and Kirrel3, did not significantly change after ectopic AP-

337 2ε expression. In fact, by immunostaining against Robo2 and Nrp2 we confirmed
338 immunoreactivity of Nrp2 in the anterior and Robo2 in the pAOB similar to controls and
339 observed no significant differences in the average size of anterior or posterior AOB
340 between genotypes (Figure S6 A,B,E). Moreover, quantifications based on Kirrel2 and
341 Kirrel3 immunostaining did not reveal major changes in glomerular size or number in the
342 AOB (Figure S6C,D,F,G) (Bahreini Jangjoo et al., 2021).
343

344 **Ps6 immunostaining reveals that OMPCre$^{+/-}$/R26AP-2ε$^{+/-}$ mutants have defective**
345 **response to female urines.**

346 Whole male mouse urine activates both V1Rs and V2Rs (Krieger et al., 1999),
347 while female odorants mostly activate apical VSNs (Dudley and Moss, 1999; Kimoto et
348 al., 2005; Norlin et al., 2001; Silvotti et al., 2018). To determine if OMPCre$^{+/-}$/R26AP-2ε$^{+/-}$
349 mice had altered chemodetection, we quantified VSNs' activation after exposure of
350 control and mutant mice to either male or female soiled bedding. Brains were collected
351 after 90 minutes of exposure to the soiled bedding, to allow adequate time for the
352 phosphorylation of the ribosomal protein S6 (pS6) in the VSNs' cell bodies (Silvotti et al.,
353 2018). VSNs activation was quantified after immunostaining against pS6 (Ser 240/244)
354 on coronal sections of the VNO (Figure 6A-D). Apical and basal VSNs were identified with
355 immunostaining against Meis2 and categorized as either pS6+/Meis2+ apical or
356 pS6+/Meis2- basal VSNs (Figure 6A-D). When exposed to male bedding we observed
357 that OMPCre$^{+/-}$/R26AP-2ε$^{+/-}$ mice had a lower average number of activated apical VSNs
358 compared to controls, however this difference was non statistically significant (Figure
359 6A,B,E). Although this difference was non statistically significant, we did find a significant
360 reduction in the total activation of VSNs in female mutants.

361 In order to further analyze the activity of apical VSNs we exposed control and
362 OMPCre$^{+/-}$/R26AP-2ε$^{+/-}$ males and females to female soiled bedding which mostly
363 activates apical VSNs. This experiment highlighted a dramatic reduction in apical VSNs'
364 activation, as well as total activation of VSNs (pS6+/Meis2+) of mutant mice for both
365 sexes (Figure 6C,D,F).
366

367 **Ectopic AP-2ε enhances intermale aggressive behavior but not preference for**
368 **opposite sex odorants.**
369 To determine whether the aberrant gene expression in apical VSNs could alter
370 VSNs' functions and related social behaviors, we evaluated intermale aggression and
371 odorant preference (Koolhaas et al., 2013). By performing resident intruder tests, we
372 showed that the level of intermale aggression of OMPCre$^{+/-}$/R26AP-2ε$^{+/-}$ male mice was
373 higher but not significantly different than controls (P=0.051) (Figure 6G). However, among
374 the animals that displayed aggressive behavior we observed significant increase in the
375 number of attacks from WT to OMPCre$^{+/-}$/R26AP-2ε$^{+/-}$ mutants (p=0.0015; WT=16.00
376 SE+/- 3.1; Ectopic=43.75 SE+/- 4.8).
377 The sex urines preference test revealed that both male and female OMPCre$^{+/-}$
378 /R26AP-2ε$^{+/-}$ mutants exhibited preferential interest in opposite sex urines similar to
379 controls (Figure 6H). Interestingly, OMPCre$^{+/-}$/R26AP-2ε$^{+/-}$ females, displayed much more
380 variability in their individual odor preferences compared to controls, nonetheless the
381 ectopic mutants still retained their preference for opposite sex odorants.
382 All together these data suggest that ectopic AP-2ε expression decreases apical VSNs'
383 functionality (Figure 6A-F) likely leading to an increase in aggression behavior but not
384 compromising opposite sex odorants preferences (Figure 6G,H). These data are in line
385 with previous findings indicating that loss of apical VSN signal transduction enhances
386 territorial aggression in males without substantial changes in sex odor preferences
387 (Trouillet et al., 2019).
388
389 **The negative effects of ectopic AP-2ε expression in apical neurons functionality is**
390 **reflected by reduced c-Fos activation in the anterior AOB.**
391 To further investigate if AP-2ε ectopic expression in apical neurons alters the
392 vomeronasal signal transduction, we analyzed c-Fos activation in the AOB. To do this we
393 analyzed the AOBs of control and OMPCre$^{+/-}$/R26AP-2ε$^{+/-}$ animals exposed to opposite
394 sex soiled bedding. This analysis revealed that c-Fos activation in the aAOB was
395 statistically different only after exposure to female soiled bedding (Figure 6I,K), while
396 there was a non-significant reduction in c-Fos activation in the aAOB of female OMPCre$^{+/-}$
397 /R26AP-2ε$^{+/-}$ mice exposed to male bedding when compared to wildtypes (Figure 6J).

398 These data suggest that ectopic AP-2ε expression reduces the functionality of the V1R
399 VSNs projecting to the aAOB but does not alter the functionality of basal VSNs.
400
401 **Identification of direct AP-2ε targets via CUT&RUN**
402 Our findings suggest a key role for AP-2ε in controlling the expression of specific
403 basal specific/enriched genes. Transcriptomic studies in AP-2ε^{Null} mice showed loss of
404 expression of basal VSN specific genes suggesting that AP-2ε controls parts of the basal
405 and apical VSN genetic programs (Lin et al., 2018). However, it remains unknown
406 whether AP-2ε regulates VSN genetic programs directly or indirectly. So, we performed
407 genome-wide mapping of transcription factor occupancy with cleavage under targets and
408 release using nuclease (CUT&RUN) to determine the direct genetic targets of AP-2ε in
409 the VNO to pair with our scRNA-Seq (Figure 7H-K). Our analyses identified over 5025
410 replicable peaks in VNO tissue indicating AP-2ε binding sites. Notably, performing
411 CUT&RUN and sequencing from AP-2ε KOs revealed 203 peaks, of which 154
412 overlapped with called WT peaks. After subtracting out peaks called in the knockout, we
413 were left with 4871 peaks (Figure 7H). AP-2e peaks of the WT were assigned to 3186
414 genes. None of the peaks of the AP-2ε KO that were subtracted out were associated with
415 apically or basally enriched genes. CUT&RUN peaks of ectopic mutants were largely
416 similar to that of WTs (Figure 7H).
417 Of these putative binding sites, we found that 60.23% of the peaks occurred in
418 promoter regions (defined as any region 1000bp upstream or 200bp downstream a
419 transcription start site), 18.6% in distal intergenic regions, and ~17.56% in intronic regions
420 (Figure 7I). These results suggest that most AP-2ε activity directly regulates transcription,
421 with perhaps a secondary role in enhancer regions.
422 Gene Ontology analysis of genes associated with AP-2ε peaks showed an
423 enrichment of factors involved in protein degradation, transcription coregulator activity,
424 and histone and chromatin modification (Figure S7A). Motif enrichment analysis of AP-2ε
425 peaks revealed Tfap2 as the top enriched motif (p=1e-180), as expected. Other
426 transcription factor motifs enriched in the same regions as AP-2ε peaks include SP, KLF,
427 EBF, RFX, NRF, DLX, and LHX transcription factor families (Figure S7B). As many
428 transcription factors work with other cofactors to regulate gene expression (Huang et al.,

429 2015; Monahan et al., 2017), these motifs may represent potential cofactors that work in
430 concert with AP-2ε to mediate either an activating or repressive role in the VNO.
431 When we compared AP-2ε direct targets with our identified apical and basal
432 enriched genes from mature VSN populations, we discovered that 18% of our identified
433 apical-enriched genes (5/27 genes) (Supplementary Table 1) were AP-2ε direct targets
434 and approximately 47% of our identified basal-enriched genes (21/50 genes) are AP-2ε
435 direct targets (Figure 7J). Of the most canonical apical and basal markers and signal
436 transduction machinery only Gαi2/Gnai2 had putative direct AP-2ε occupancy and
437 assumed regulation of transcription (Figure S7C). Out of our newly discovered list of basal
438 enriched genes (Supplementary Table 1) we identified that Krt18 has a putative AP-2ε
439 binding site within its promoter region. As expected from a terminal selector gene, these
440 data suggest that AP-2ε directly binds and regulates batteries of apical and basal
441 enriched genes (Figure S7C).
442 These data suggest that AP-2ε plays a dual role in maintaining the basal VSNs'
443 genetic program while restricting the expression of genes normally enriched in apical
444 VSNs (Figures 7J,K; S7). In line with this, CUT&RUN from ectopic expressors gave tracks
445 that largely overlapped with those of the WT controls (Figure S7) (Figure 7H). However,
446 when plotting the signals at the promoter of apical and basal enriched genes for WT, AP-
447 2ε KO and AP-2ε ectopic expressors we observed more signal at the apical-enriched
448 promoters in the ectopic mice dataset (Figure S7D). This data suggests that ectopic
449 expression of AP-2ε in apical neurons facilitates its access to the promoter of apical
450 enriched genes as these are normally active in the apical neurons.
451
452
453 **DISCUSSION**
454 Understanding how differentiated neurons retain cellular plasticity remains critical
455 to identify how genetic insults can compromise neuronal identity, circuit assembly and
456 function (Hobert and Kratsios, 2019; Molyneaux et al., 2007; Patel and Hobert, 2017;
457 Pereira et al., 2019; Rahe and Hobert, 2019). Spatial and temporal expression of terminal
458 selector genes regulates the establishment and maintenance of neuronal identity remains

459 foundational to elucidate the assembly of functional neuronal circuits (Arlotta et al., 2005;
460 Cau et al., 2002; Cau et al., 1997; Molyneaux et al., 2007). In fact, loss of terminal selector
461 genes can lead to loss of neuronal identity and increase cellular/phenotypic plasticity,
462 while expression of specific TFs can induce specific cellular features only at particular
463 developmental windows (Hobert, 2008; Rahe and Hobert, 2019).

464 Rodents and some marsupials have a binary vomeronasal epithelium where the
465 two main types of VSNs, apical and basal VSNs, are generated throughout life from a
466 common pool of Ascl1 progenitors (Berghard and Buck, 1996; Jia and Halpern, 1996;
467 Katreddi and Forni, 2021; Mohrhardt et al., 2018; Silva and Antunes, 2017; Taroc et al.,
468 2020; Weiler et al., 1999). The generation of these two distinct populations is central for
469 critical socio-sexual behavior in rodents (Oboti et al., 2014; Perez-Gomez et al., 2014). In
470 a recent study we have shown that the apical-basal differentiation dichotomy of VSNs is
471 dictated by Notch signaling. The transcription factor TF AP-2ε is expressed in maturing
472 cells fated to become V2R neurons. In this study, we combined scRNA-Seq, histology,
473 behavior, and CUT&RUN methodologies to test if TF AP-2ε is a basal VSN specific
474 terminal selector gene capable of partially reprogramming the apical VSN identity.

475 Using scRNA-Seq, we discovered key transcriptomic differences between mature
476 basal and apical VSNs that were previously unreported (Figure 1Q, Supplementary Table
477 S1). We also confirmed that AP-2ε mRNA is restricted to maturing Gαo/basal VSNs
478 (Figure 1K) and that AP-2ε itself does not initiate the basal VSN differentiation program,
479 but rather maintains the integrity of the basal neuronal identity. In fact by re-expressing
480 AP-2ε in AP-2ε KOs we demonstrated that AP-2ε is indispensable for basal cellular
481 homeostasis (Figure 2) and therefore for the establishment of normal territorial and sex-
482 preference behaviors of rodents (Figure 3). We also elucidated that AP-2ε acts in
483 controlling VSN gene expression through activating and repressive activity when
484 analyzing mature/maturing Meis2+ apical VSNs in OMPCre$^{+/-}$/R26AP-2ε$^{+/-}$ mutant mice
485 (Figure 7).

486 During differentiation chromatin barriers dynamically restrict the cellular plasticity,
487 preventing ectopic terminal selector genes from genetically reassigning neurons (Rahe
488 and Hobert, 2019). We have previously shown that postmitotic VSNs of AP-2ε KO mice
489 can partially deviate from the basal differentiation program and turn on sets of apical

490 specific genes. However, AP-2ε LOF did not prevent basal neurons from acquiring basal
491 features, such as Gαo or V2Rs ((Lin et al., 2018), suggesting that AP-2ε activity is crucial
492 to restrict basal VSN phenotypic plasticity rather than establishing the basal cell fate (Lin
493 et al., 2018). Here we showed that AP-2ε null mice have reduced odorant sex preference
494 and intermale aggressive behavior, which are classic phenotypes related to basal VSN
495 LOF (Stowers et al., 2002). However, we found that reintroducing AP-2ε in maturing basal
496 AP-2ε KO neurons was sufficient to rescue cellular homeostasis (Figure 2), physiological
497 functions, and related behavior (Figure 3).
498 Terminal selectors define neuronal identity by suppressing alternative programs
499 and can also act as pioneer factors (Lupien et al., 2008; Magnani et al., 2011; Mangale
500 et al., 2008). Based on our rescue data, we propose that AP-2ε can partially
501 reprogram/alter the transcriptome of differentiated cells, as expected from a pioneer factor
502 and other members of the Tfap2 family (Rothstein and Simoes-Costa, 2020).
503 When we used OMPCre drivers to induce ectopic AP-2ε in differentiated olfactory
504 and both apical and basal vomeronasal neurons, we observed progressive gene
505 expression, and morphological changes in the VNO, but no gross morphological changes
506 in the main olfactory epithelium (Figures 4; 5; S2). We suspect the lack of phenotype in
507 the OE may arise from the absence of necessary Tfap2 cofactors , that are expressed in
508 the VNO (Figure S1) (Eckert et al., 2005).
509 The co-expression of AP-2ε in Meis2+ apical VSNs in OMPCre$^{+/-}$/R26AP-2ε$^{+/-}$ mice
510 revealed that Meis2, and most apical specific genes, were expressed at P10 (Figure 7C).
511 However, single-cell transcriptome analyses in adult AP-2ε ectopic mice indicated that
512 several apical genes, including Meis2, were expressed at significantly lower levels than
513 controls (Figure S8A,C). These data suggest that AP-2ε can negatively modulate genes
514 enriched in the apical program.
515 Ectopic expression of individual terminal selector genes can selectively control
516 specific molecular features linked to neuronal function and identity, but not pan-neuronal
517 features like guidance cue receptors (Patel and Hobert, 2017; Stefanakis et al., 2015).
518 Our ScRNA-Seq revealed that AP-2ε ectopic expression, does not alter the expression
519 of VSN-specific guidance cue receptors Nrp2 and Robo2 (Cho et al., 2011; Cloutier et al.,

520 2002; Prince et al., 2009; Walz et al., 2002). Notably Nrp2 and Robo2 start to be
521 expressed soon after the apical/basal VSNs' developmental trajectories are established,
522 suggesting that these genes are expressed before and independently of tfap2e
523 expression (Figures 1; 7; S6). In line with this, we observed that AP-2ε ectopic expression
524 did not significantly change Kirrel2 and Kirrel3 expression patterns (S6). As a result we
525 found not significant changes in glomeruli size or number in the AOB (S6C,D,F,G).

526 In OMPCre$^{+/-}$/R26AP-2ε$^{+/-}$ mutants, we observed that the cellular organization and
527 lamination of the vomeronasal epithelium became severely disrupted between P10 and
528 adult ages (Figure 5). In fact, in the mutants, we found basal neurons located at the level
529 of the VNE lumen and ectopic sustentacular cells forming intraepithelial cyst-like
530 structures in both apical and basal territories (Figure 5B,C). Notably, the disorganization
531 of the VNE that resembles intraepithelial cysts as previously described in aging mice
532 (Wilson and Raisman, 1980), appeared to be more pronounced/frequent in regions
533 proximal to the neurogenic marginal zones (Figure 5D,E), where OMP mRNA is
534 expressed following Gap43 expression. Therefore, we posit that the regionalization of the
535 VNE phenotypes might represent cells that underwent AP-2ε ectopic expression at early
536 maturation stages. When we compared mRNA of control and ectopic AP-2ε mutants,
537 which have disorganized VNE, we observed changes in expression levels of many
538 surface and cell adhesion related molecules as well as upregulation of stress related
539 genes (Figures 5E; S3E). In addition to this, scRNA-seq analysis of AP-2ε positive and
540 negative sustentacular cells in adult OMPCre$^{+/-}$/R26AP-2ε$^{+/-}$ mutants revealed massive
541 changes in gene expression in these support cells. Future studies should focus on
542 understanding which of the dysregulated genes in VSNs and sustentacular cells
543 contribute to the cytoarchitectural organization of VSNs and sustentacular cells.

544 Sex odorants activate different sets of vomeronasal receptors and therefore
545 different populations of VSNs (Dudley and Moss, 1999; Keller et al., 2006; Silvotti et al.,
546 2018). Interestingly, scRNA-seq analysis and validation via RNA scope and ISH revealed
547 that ectopic AP-2ε in mature apical VSNs leads to the upregulation of basal enriched
548 genes such as Gao (Figure 4) and the ER chaperone protein Calreticulin-4 (Calr4) (Figure
549 7). In the ectopic AP-2ε mutants we observed a reduction in mRNA of Calr (Figure 7D).
550 Loss of Calr expression has been previously shown to increase V2R cell surface

551 expression (Dey and Matsunami, 2011). Changes in Calr4 and Calr expression levels
552 could be partially responsible for the overall increase in family-C V2Rs cell surface
553 expression/immunoreactivity (Dey and Matsunami, 2011) observed in ectopic AP-2ε
554 mutants (Figure 4C,F,H).

555 After OMPCre driven ectopic AP-2ε expression we observed a significant
556 upregulation of mRNAs of V2r receptors coded by genes belonging to the C-family
557 (Silvotti et al., 2011) (Figure S2). Notably, our data suggest that some apical neurons of
558 controls can express low mRNA levels of family-C Vnm2r mRNAs (Figures 4; S2E-H).
559 These data suggest that some family-C genes (e.g. Vmn2r7), which are known to not
560 follow rigorous mechanisms of monogenic expression, might also have a much looser
561 cell type specific expression control that previously postulated. However, using the anti
562 V2R2 antibody, which recognized a large spectrum of Vmn2r of the family-C, including
563 Vmn2r7 (Silvotti et al., 2011), we could detect cells immunoreactive for both V2R2 and
564 Meis2 in AP-2ε ectopic mutants (Figure 4L). This suggests that in control animals apical
565 VSNs either express V2R genes below immune-detectability (Fig 4K) or that post
566 transcriptional mechanisms may play roles in silencing translation.

567 Using pS6 immunoreactivity to detect activated VSNs, and cFos to detect signal
568 transduction in the AOB revealed that ectopic AP-2ε mutants have an overall decreased
569 apical cells' ability to detect and transduce signal to the aAOB (Figure 6). Notably these
570 defects resulted more obvious, in both males and females, after female bedding exposure
571 (Figure 6). Conditional ablation of normal apical VSN signal transduction does not
572 undermine intermale aggression, rather it enhances territorial aggression in mutant males
573 (Trouillet et al., 2019). In line with this, we found that OMPCre$^{+/-/}$R26AP-2ε$^{+/-}$ mutants that
574 display aggressive behavior had higher levels of aggression towards male intruders when
575 compared to WT controls (Figure 6G). These data indicate that ectopic AP-2ε expression
576 in V1R neurons is sufficient to partially subvert their function and therefore alter intrinsic
577 social behaviors.

578 In rodents, olfactory sex discrimination persists after VNO excision; however,
579 preference for opposite sex odorants is mediated by the accessory olfactory system
580 (Keller et al., 2006; Pankevich et al., 2004). Despite the partial desensitization of the
581 apical VSNs in OMPCre$^{+/-/}$R26AP-2ε$^{+/-}$ mutants, transcriptome, and morphological

582 changes in the VNO did not compromise normal sex odorant preference in male or female
583 mutants. In fact, conditional ablation of Gαi2, which is required for normal signaling of
584 apical VSNs, did not alter normal male sexual behavior, including male preference for
585 estrous female urine (Trouillet et al., 2019). Our data support a dispensable role for apical
586 VSNs neurons in the tested sexual behavior behaviors (Figure 6C,D,H).

587 To elucidate the mechanism of action of AP-2ε, we performed CUT&RUN (Skene
588 et al., 2018; Skene and Henikoff, 2017). This analysis (Figure 7) identified putative direct
589 targets of AP-2ε and showed 3000+ putative binding sites in the vomeronasal tissue. The
590 specificity of binding was confirmed by CUT&RUN experiments on AP-2ε Kos (Figure
591 7H). In the identified AP-2ε target genes we found that most of binding sites were primarily
592 in promoter regions, not in intergenic and intronic regions. These data suggest that AP-
593 2ε's main mechanism of action directly regulates gene transcription with perhaps a
594 secondary role at enhancer regions. We found AP-2ε bound to the up and down-regulated
595 genes in both apical VSNs and sustentacular cells in the OMPCre$^{+/-}$/R26AP-2ε$^{+/-}$ ectopic
596 mouse line, which suggests that AP-2ε can act as both a transcriptional activator and
597 repressor. Motif analysis of these up and downregulated regions indicates that AP-2ε may
598 function in concert with specific transcriptional cofactors to fulfill a dual role in maintaining
599 the basal VSN genetic program and restricting cellular plasticity (Figure S7). Notably our
600 CUT&RUN data showed an enrichment of factors involved in transcription coregulator
601 activity, histone modification, and chromatin modification (Figure S7A). These data
602 indicate that AP-2ε may play a role in modifying the chromatin landscape indirectly or in
603 tandem with these transcriptional cofactors to regulate the basal genetic program. Even
604 though transcriptome and histological analysis of the VNE showed significant changes in
605 canonical apical and basal specific genes, we only Gαi2 and Krt18 had AP-2ε peak
606 assignments, suggesting that AP-2ε acts indirectly to regulate these genes. However,
607 since peaks were assigned to the nearest gene, we cannot exclude long-distance gene
608 regulation through enhancer regions as a contributor. CUT&RUN peaks of ectopic
609 mutants were largely similar to that of WTs, while only background peaks were found in
610 AP-2ε KOs. Notably, our data suggests that ectopic expression of AP-2ε in apical neurons

allows for access of Tfap2e to the promoter of apical enriched genes as they are in the euchromatic state (S7).

In conclusion, the results of our study indicate that AP-2ε has some features of a terminal selector gene. In fact, AP-2ε plays roles in controlling the expression or expression levels of several basal enriched VSN genes and repressing apical ones, which is necessary for normal basal VSN functions that mediate territorial and sex preference behaviors in mice. We recently found that the establishment of the apical/basal identity is a slow and multistep process, and that the apical/basal identity is primarily established by Notch signaling as soon as the cells become postmitotic (Katreddi et al., 2022). In line with this, we observed that after ectopic AP-2ε expression in maturing apical neurons the core of their default apical identity is maintained, however some of the genes normally expressed in alternative basal identity are turned on in apical neurons. Our data suggest that after AP-2ε expression the apical VSNs acquire an ambiguous transcriptome identity as ectopic AP-2ε expression is sufficient to bypass some layers of cellular plasticity restrictions over time. These changes translate into a reduced functionality of the apical neurons, rather than into a transdifferentiation to basal VSNs. The genetic changes induced by ectopic AP-2ε further manifest in a progressive disorganization of the vomeronasal neuroepithelium like that reported in aging animals (Wilson and Raisman, 1980).

Our study suggests that as previously hypothesized by others (Hobert and Kratsios, 2019; Rahe and Hobert, 2019) aberrant expression of terminal selector genes in postnatal neurons can alter the transcriptomic identity of neurons, organization neuroepithelia, and potentially lead to neuropathologies.

ACKNOWLEDGEMENTS

Funding

This publication was supported by the National Institutes of Health (NIH) by the Eunice Kennedy Shriver National Institute of Child Health and Human Development of the National Institutes of Health under the Awards R01-HD097331/HD/NICHD (P.E.F), the National Institute of Deafness and Other Communication Disorders of the National

642 Institutes of Health under the Award R01-DC017149 (P.E.F), the National Institute of
643 Dental and Craniofacial Research under the Award R01DE028576 (M.S.-C), and the
644 National Institute of Mental Health under the Award R15-MH118692 (D.G.Z).
645
646
647 **STAR★METHODS**
648

Key Resources Table

REAGENT or RESOURCE	SOURCE	IDENTIFIER
Antibodies		
active-Cleaved Caspase 3 (CC3)	Millipore	AB3623
Gnao1 (Gao)	Invitrogen	PA5-59337
Gnao1 (Gao)	Synaptic Systems	271 111
Keratin 18	Abcam	ab52948
Ki67	Millipore	AB9260
Ki67 (Clone #8D5)	Cell Signalling Technology	9449S
Kirrel2/NEPH3	R&D Systems	AF2930
Kirrel3/NEPH2	NeuroMab	75-333
Meis2	Santa Cruz	sc-81986
Meis2	Abcam	ab73164
Neuropilin-2 (Nrp2)	R&D Systems	AF567
Olfactory Marker Protein (OMP)	WAKO	54410001
Pecam1/CD31	BD Pharmingen	557355
Phospho-S6 Ribosomal Protein (Ser240/244)	Cell Signaling Tech	D68F8
Robo2	Santa Cruz	sc-376177
Sox2	R&D Systems	AF2018
Tfap2e (AP-2ε)	R&D Systems	AF5060
Tfap2e (AP-2ε)	Santa Cruz	sc-131393 X
Tfap2e (AP-2ε)	ProteinTech Group	25829-1-AP
Tmem16a/Ano1	Abcam	ab53212
V2R2	Roberto Tirindelli (University of Parma)	
a-chicken (Alex488)	Jackson Labs	703-545-155
a-chicken (biotinylated)	Vector	ba9010

a-goat (Alexa488)	Molecular Probes	a11055
a-goat (Alexa594)	Molecular Probes	a11058
a-goat (biotinylated)	Vector	ba9500
a-mouse (Alexa488)	Molecular Probes	a21202
a-mouse (Alexa594)	Molecular Probes	a10037
a-mouse (biotinylated)	Vector	ba2000
a-rabbit (Alexa488)	Molecular Probes	a21206
a-rabbit (Alexa594)	Jackson Labs	711-585-152
a-rabbit (biotinylated)	Vector	ba1100
Chemicals and Kits	**Source**	**Identifier**
Neuron Isolation Enzyme (with papain)	Thermo Fisher	Cat# 88285
Neurobasal Medium	Thermo Fisher	Cat# 21103049
Dimethyl sulfoxide (DMSO)	Sigma-Aldrich	Cat# 472301
Fetal Bovine Serum	Thermo Fisher	Cat# 26140079
Diaminobenzidine (DAB)	Sigma	Cat# D9015-100MG
DAPI	CALBIOCHEM	Cat# 268298
DIG Labelling Kit	Roche	Ref# 11 175 025 910
DIG Detection Kit	Roche	Ref# 11 175 041 910
37% Formaldeyde	Sigma	Cat# F1635-500ML
Tissue-Tek O.C.T. Compound	VWR	Cat# 25608-930
ABC HRP Kit	Vector	Cat# PK-6100
Bovine Serum Albumin	Thermo-Fisher	Cat# CP9703-100
Fluorogel Mounting Media	Electron Microscopy Sciences	Cat# 17985-11
Sub-X Mounting Medium	Electron Microscopy Sciences	Cat# 1351g
Sahara Hot Start Taq	Chai	Cat# R02151S
NEBNext Ultra II DNA Library Prep Kit for Illumina	New England Biolabs	Cat# E7645

Experimental Model: Mouse Strains	**Source**	**Identifier**
AP2eCre	Trevor Williams (University of Colorado, Denver)	
B6;129P2-Omptm4(cre)Mom/MomJ	Jackson Labs	Stock No: 006668
B6.Cg-Gt(ROSA)26Sor tm(CAG-mTfap2e)For (R26AP2e)	This Paper	
Software and Algorithms	**Source**	**Identifier**
FIJI ImageJ software (Version 2.1.0/1.53c)	NIH	https://imagej.nih.gov/ij/
GraphPad Prism 9 software	GraphPad	https://www.graphpad.com/
Photoshop CC 2020	Adobe	https://www.adobe.com/products/photoshop.html
RStudio (Version 1.3.1073)	RStudio	https://rstudio.com/
R version 4.0.2	The R Project	https://www.r-project.org/
Seurat 4.0.5	Satija Lab	https://satijalab.org/seurat/
ButtonBox v.5.0	Behavioral Research Solutions, LLC	
Cutadapt	Martin 2011	https://cutadapt.readthedocs.io/en/stable/
Bowtie 2	Langmead and Salzberg 2012	http://bowtie-bio.sourceforge.net/bowtie2/index.shtml
MACS2	Zhang, Liu et al. 2008	https://chipster.csc.fi/manual/macs2.html
ChIPseeker	Yu, Wang et al. 2015	https://bioconductor.org/packages/release/bioc/html/ChIPseeker.html

clusterProfiler	Yu, Wang et al. 2012	https://bioconductor.org/packages/release/bioc/html/clusterProfiler.html
HOMER	Benner Lab	http://homer.ucsd.edu/homer/
Deposited Data	**Source**	**Identifier**
P60 WT scRNA-Seq_Forni01b	Forni Lab	GSE190330
P10 and P90 OMPCreR26AP2e Data	Forni Lab	GSE192746
Tfap2e CUT&RUN Data	Simoes-Costa Lab	GSE193139
Oligonucleotides	**Source**	**Identifier**
GGA GGG GGG CTCT GAG AT	This Paper	R26-AP2e Common
GGC TGG TGT GGC CAA TGC	This Paper	R26-AP2e Mutant
GTC GTG AGG CTG CAG GTC	This Paper	R26-AP2e WT
AGT TCG ATC ACT GGA ACG TG	Jackson Labs	OMP WT Fwd
CCC AAA AGG CCT CTA CAG TCT	Jackson Labs	OMP WT Rvs
TAG TGA AAC AGG GGC AAT GG	Jackson Labs	OMP Mutant Fwd
AGA CTG CCT TGG GAA AAG CG	Jackson Labs	OMP Mutant Rvs
GCT GGT GAG TCA ACC TGC CTG CAG	Trevor Williams (University of Colorado, Denver)	AP2e WT AK19
GGT CAC CTT GTA CTT GGA TGT TGA G	Trevor Williams (University of Colorado, Denver)	AP2e WT AK20
AGG TGT AGA GAA GGC ACT TAG C	Jackson Labs	Cre Fwd
CTA ATC GCC ATC TTC CAG CAG G	Jackson Labs	Cre Rvs

GCGGCTACGTGAAGCTGTTT CCGAGTGGCTTGGACCAGAA GGACATGCATGGAGACTCAG AATATAACATCATGTTTGGTC CGGACATCTGCGGTCCTGGC ACCAAGAAGGTTCATGTCATC TTTAACTACAAGGGCAAGAAT GTGCTGATCAACAAGGATAT CCGGTGTAAGGATGATGAAT TCACACACCTATACACACTGA TTGTGCGGCCAGACAACACC TATGAGGTGAAAATTGACAAC AGCCAGGTGGAGTCAGGCTC CTTGGAGGATGATTGGGACT TTCTGCCACCCAAGAAGATAA AGGACCCTGATGCTGCCAAG CCGGAAGACTGGGATGAACG AGCCAAGATCGATGACCCCA CAGATTCCAAGCCTGAGGAC TGGGACAAGCCAGAGCACAT CCCTGACCCTGATGCTAAGA AGCCTGAGGACTGGGATGAA GAGATGGATGGAGAGTGGGA ACCACCAGTGATTCAAAATCC TGAATACAAGGGCGAGTGGA AACCACGTCAAATTGACAACC CAGATTACAAGGGTACCTGG ATACACCCAGAAATTGACAAC CCTGAATACTCCCCCGATGC AAATATCTATGCCTATGATAG TTTTGCTGTACTGGGCCTAGA TCTCTGGCAGGTCAAGTCCG GGACAATCTTTGACAATTTCC TCATCACCAATGATGAGGCC TATGCAGAGGAGTTTGGCAA TGAGACGTGGGGTGTTACCA AGGCTGCAGAGAAGCAGATG AAGGACAAGCAGGATGAGGA GCAGAGGCTTAAGGAAGAAG AAGAGGACAAGAAGCGTAAA GAGGAAGAAGAAGCTGAGGA TAAAGAGGATGATGATGACA GAGATGAAGATGAGGATGAA GAAGATGAGAAGGAGGAAGA	This Paper	Probe against Calreticulin

TGAGGAAGAATCCCCTGGCCAA		

TGGGATGAACGACAACAGAT AGAGGATCCTGACGATAAGA AACCTGAGGACTGGGAGGAC TCTGAATTCATCCCAGACCCG GATGCCAAGAAGCCAGATGA CTGGAATGAGGCGATGGATG GAGTGTGGGAAGGGCCCTTG ATACCAAACGTCAAGTACATG GGAGAATGGAAACCTCGGAT CATTGACAACCCCAATTACCA GGGCGAGTGGATTCACCCAG AGATAGACAACCCCAAATAC AGGCCTGACCCCACCATTGGT CACTATCACAACATTAGTGTC CTTGGTCTGGATCTTTGGCAG GTGAAATCAGGCAGCATCTTT GACAATTTCCTTCTAACAAAT GATGAAGAGTTTGCTGAAGA GGTTGGAAATATGACCTGGG GATTAAGAAAGGATGTGGAG CAGCAGTGGAGAGAGCTGTA TGAGGAAATGGAGAAACAGA AGGAGGCGGAGGAGACCAAG AAGAAGAGGGAAAAGGAGAG AGCCAGGCAAGAGGACGTCT GGGGACTAGATGAGGAGGAT GAGGAGGACGCTGAAGAGGA CGACGAGGAGGAAGCAGAGG AAAGGCTCAAGCAGGAAGGC AGTGCAGCGAGGGCGTCTCTG GACCAGAAGGAAGCCCACTT GGATCAGAAGGATGAACTGT AACTGCACAGACACTGGGTGT GGCCGAAGTCAGAGACGGTG CTTAGAGAGGGAAATGGGCC CTCGCTTAGCAAATTATGGGA AGTAAAACGACTCATTCTTTT TAGATAAACTTTGGATTTATA GTTCTACTCCCCTTCCCTGCTC TA	This Paper	Probe against Calreticulin4

654 **RESOURCE AVAILABILITY**

655 ***Lead contact***

656 Further information and requests for resources and reagents should be directed to
657 and will be fulfilled by the lead contact, Paolo E. Forni (pforni@albany.edu).

658

659 ***Materials availability***

660 Mouse lines generated in this study will be deposited to Jackson Labs by the time
661 of publication.

662 There are restrictions in availability of the antibody Rabbit anti-V2R2 which was
663 obtained from the lab of Dr. Roberto Tornielli (University of Parma, Italy) and is not
664 commercially available.

665

666 ***Data and code availability***

667 The Single-cell RNA-sequencing and CUT& RUN sequencing data discussed in
668 this publication have been deposited at NCBI's Gene Expression Omnibus and are
669 publicly available as of the date of publication. Accession numbers are listed in the key
670 resources table. This paper reports no original code. Any additional information required
671 to reanalyze the data reported in this paper is available from the lead contact upon
672 request.

673

674 **EXPERIMENTAL MODEL AND SUBJECT DETAILS**

675

676 ***Animals***

677 The R26AP2ε mice were produced by Cyagen (Santa Clara, CA). on a C57B/6
678 background. The AP-2εCre line (*Tfap2e*$^{tm1(cre)Will}$) was obtained from Dr. Trevor Williams,
679 Department of Craniofacial Biology, University of Colorado. The R26AP-2ε (B6.Cg-
680 Gt(ROSA)26Sor$^{tm(CAG\text{-}mTfap2e)For}$) mouse line was produced through Cyagen on a C56BL/6
681 background. The OMPCre line (B6;129P2-*Omp*$^{tm4(cre)Mom}$/MomJ) was obtained from Dr.
682 Paul Feinstein (Hunter College, City University of New York) on a 129P2/OlaHsd
683 background and backcrossed to a C57BL/6 background for 6 generations at the time of
684 this study. The characterization and comparison of the rescue of the AP-2ε phenotype

685 (AP-2εCreR26AP-2ε), AP-2ε KO, and wild-types were performed on a C57BL/6
686 background. OMPCre$^{+/-}$/R26AP2ε$^{+/-}$ mutant mice are viable. Genotyping of mutants was
687 performed by PCR. Primers used are detailed in the Key Resources Table.
688 Mice were housed under a 12hr day/night cycle. Animals were collected/analyzed
689 at P10, P21, and Adult (P60-P90) ages. For all morphological analyses both males and
690 females were included unless otherwise specified. All mouse studies were approved
691 by the University at Albany Institutional Animal Care and Use Committee (IACUC). Mouse
692 lines generated in this study will be deposited to Jackson Labs by the time of publication.
693
694 **METHOD DETAILS**
695 ***Generation of the AP-2ε conditional Knock-In Model***
696 The AP-2ε conditional Knock-In allele was generated by targeting the ROSA26
697 gene in C57BL/6 ES cells. The "CAG-loxP-stop-loxP-mouse Tfap2e CDS-polyA" cassette
698 was cloned into intron 1 of ROSA26 in the reverse orientation. In the targeting vector, the
699 positive selection marker (Neo) was flanked by SDA (self-deletion anchor) site, and DTA
700 was used for negative selection. Mouse genomic fragments containing homology arms
701 (Has) were amplified from BAC clone by using high fidelity Taq DNA polymerase and
702 were sequentially assembled into a targeting vector together with recombination sites and
703 selection markers.
704 The ROSA26 targeting construct was linearized by restriction digestion with AscI
705 followed by phenol/chloroform extraction and ethanol precipitation. The linearized vector
706 was transfected into C57BL/6 ES cells according to Taconic-Cyagen's standard
707 electroporation procedures and G418 resistant clones were selected for 24 hours post-
708 electroporation. These were then screened for homologous recombination by PCR and
709 characterized by Southern Blot analysis. Two separate clones, A2 and H2, were
710 successfully transmitted to germline and characterized.
711 Genotyping for the R26AP-2ε mouse line was performed by PCR using R26-AP-
712 2e Common (5' GGAGGGGGGCTCTGAGAT 3'), R26-AP-2ε Mutant (5'
713 GGCTGGTGTGGCCAATGC 3'), R26-AP-2ε WT (5' GTCGTGAGGCTGCAGGTC 3')
714 with expected bands at 552bp (Mutant) and 400bp (WT).
715

716 ***Both OMPCre$^{+/-}$ and wildtype mice are used as controls depending on availability***
717 ***during performed experiments.***
718 ***Resident Intruder Test***
719 The resident intruder assay was used to evaluate aggression in male mice of
720 mutants and controls. Test subjects were housed with intact females for at least one week
721 prior to testing. On the day of testing, all subjects (residents and intruders) were
722 acclimated to the experimental environment for at least 30 minutes prior to the assay.
723 Females were removed immediately before testing. Castrated C57B mice were swabbed
724 with male whole urine immediately before being introduced into the resident male's home
725 cage. Interactions between isolated residents and intruders were recorded for 10min and
726 videos were evaluated using ButtonBox v.5.0 (Behavioral Research Solutions, Madison
727 WI, USA) software for the number and duration of attacks.
728
729 ***Innate olfactory preference test***
730 Adult mice were isolated for at least one week prior to testing. Individual mice were
731 habituated to the experimental environment for at least 30 minutes, then to the test cage
732 for an additional 2 minutes. After the habituation period, cotton swabs scented with either
733 male or female whole urine was placed on either side of the test cage. The time spent
734 sniffing each odorant was normalized to total investigation time.
735
736 ***Neuronal activation in response to sex-specific odorants***
737 Adult mice were isolated for at least one week prior to exposure to either soiled
738 bedding from male or female mice for ~90min then perfused with PBS and 3.7%
739 formaldehyde in PBS, then collected to evaluate neuronal activation with
740 immunohistochemistry against pS6.
741
742 ***Tissue Preparation***
743 Tissue collected at ages ≥P10 were perfused with PBS then 3.7% formaldehyde
744 in PBS. Brain tissue was isolated at the time of perfusion and then immersion-fixed for 3-
745 4 hours at 4°C. Noses were immersion fixed in 3.7% formaldehyde in PBS at 4°C
746 overnight and then decalcified in 500mM EDTA for 3-4 days. All samples were

747 cryoprotected in 30% sucrose in PBS overnight at 4°C, followed by embedding in Tissue-
748 Tek O.C.T. Compound (Sakura Finetek USA, Inc., Torrance CA) using dry ice, and stored
749 at -80°C. Tissue was cryosectioned using a CM3050S Leica cryostat at 16μm for VNOs
750 and 20μm for brain tissue and collected on VWR Superfrost Plus Micro Slides (Radnor,
751 PA) for immunostaining and in situ hybridization (ISH). All slides were stored at -80°C
752 until ready for staining.
753
754 ***Immunohistochemistry***
755 For immunohistochemistry and immunofluorescence antigen retrieval was
756 performed on slides that were submerged in citrate buffer (pH 6.0) above 95°C for at least
757 15min before cooling to room temperature, then permeabilized with and blocked in horse
758 serum based blocking solution before transferring into primary antibodies overnight at
759 4°C. For immunohistochemistry slides were additionally incubated in an H_2O_2 solution
760 (35mL PBS+ 15mL 100% Methanol + 500μL 30% H_2O_2) after antigen retrieval.
761 For chromogen-based reactions, staining was visualized with the Vectastain ABC
762 Kit (Vector, Burlingame, CA) using diaminobenzidine (DAB) (Forni et al., 2011); sections
763 were counterstained with methyl green and mounted with Sub-X mounting medium. For
764 immunofluorescence species-appropriate secondary antibodies conjugated with either
765 Alexa Fluor 488, Alexa Fluor 594, Alexa Fluor 568, Alexa Fluor 680 were used for
766 immunofluorescence detection (Molecular Probes and Jackson ImmunoResearch
767 Laboratories, Inc., Westgrove, PA). Sections were counterstained with 4',6'-diamidino-2-
768 phenylindole (DAPI) (1:3000; Sigma-Aldrich), and coverslips were mounted with
769 FluoroGel (Electron Microscopy Services, Hatfield, PA).
770 Confocal microscopy pictures were taken on a Zeiss LSM 710 microscope.
771 Epifluorescence pictures were taken on a Leica DM4000 B LED fluorescence microscope
772 equipped with a Leica DFC310 FX camera. Images were further analyzed using
773 FIJI/ImageJ software. Antibodies and concentrations used in this study are detailed in the
774 Key Resources Table.
775
776 ***In Situ Hybridization and RNAscope***

777 Digoxigenin-labeled RNA probes were prepared by *in vitro* transcription (DIG RNA
778 labeling kit; Roche Diagnostics, Basel, Switzerland). In situ hybridizations were performed
779 on 16μm cryosections that were rehydrated in 1x PBS for 5min, fixed in 4% PFA in 0.1M
780 phosphate buffer for 20min at 4°C, treated with 10μg/mL proteinase K (Roche) for 12min
781 at 37°C, and then refixed in 4% PFA at 4°C for 20min. To inactivate the internal alkaline
782 phosphatase, the tissue was treated with 0.2M HCl for 30min. Nonspecific binding of the
783 probe to slides was reduced by dipping slides in 0.1M triethanolamine (pH 8.0)/0.25%
784 acetic anhydride solution, then washed with 2x Saline-Sodium Citrate (SSC) buffer before
785 incubating in hybridization solution for 2hrs at room temperature. Slides were then
786 hybridized with 200μl of probe in hybridization solution at 65°C overnight in a moisture
787 chamber. After hybridization, the slides were washed in 2x SSC, briefly, then in 1x
788 SSC/50% formamide for 40min at 65°C. RNase A treatment (10μg/mL) was carried out
789 at 37°C for 30min. The slides were then washed with 2x SSC then 0.2x SSC for 15min
790 each at 65°C. Hybridization was visualized by immunostaining with an alkaline
791 phosphatase conjugated anti-DIG (1:1000), and NBT/BCIP developer solution (Roche
792 Diagnostics). After color reaction, the slides were put into 10mM Tris-HCl pH 8.0/1mM
793 EDTA, rinsed in PBS and air dried before mounting with Sub-X mounting medium.
794 Single-molecule fluorescence in situ hybridization was performed using the
795 RNAscope Multiplex Fluorescence v2 assay and probes (RNAscope Probe-Mm-Abca7-
796 C4 #489021, RNAscope Probe-Mm-Gnai2 #868051, RNAscope Probe-Mm-Gnao1-E4-
797 E6-C2 #444991, Rnascope Probe-Mm-Mt3-C3 #504061, RNAscope Probe-Mm-Meis2-
798 C3 #436371) from ACDbio. The assay was performed on 16μm fixed-frozen P10-P11
799 mouse cryosections, following the manufacturer's protocol.
800
801 ***Single-Cell RNA Sequencing***
802 The vomeronasal organs of OMPCre$^{+/-}$ at P10 and OMPCre$^{+/-}$/R26AP2ε$^{+/-}$ at P10 and
803 3mo were isolated and dissociated into single-cell suspension using neural isolation
804 enzyme/papain (NIE/Papain in Neurobasal Medium with 0.5mg/mL Collagenase A,
805 1.5mM L-cysteine and 100U/mL DNAse I) incubated at 37ºC. The dissociated cells were
806 then washed with HBSS and reconstituted in cell freezing medium (90% FBS, 10%
807 DMSO). Cells were frozen from room temperature to -80ºC at a -1°C/min freeze rate.

808 Single cell suspension was sent to SingulOmics for high-throughput single-cell gene
809 expression profiling using the 10x Genomics Chromium Platform. Data were analyzed
810 along with using Seurat 4.0.5. The scRNA-seq data discussed in this publication have
811 been deposited in NCBI's Gene Expression Omnibus and are accessible through GEO
812 series accession number GSE192746
813 (https://www.ncbi.nlm.nih.gov/geo/query/acc.cgi?acc=GSE192746). We also utilized
814 previously published data from (Katreddi et al., 2022), available through GEO series
815 accession number GSE190330
816 (https://www.ncbi.nlm.nih.gov/geo/query/acc.cgi?acc=GSE190330).
817
818 ***CUT&RUN***
819 Cells frozen in 90% FBS/10%DMSO were thawed at 37°C and resuspended in
820 CUT&RUN wash buffer (20mM HEPES pH7.5, 150mM NaCl, 0.5mM spermidine, plus
821 Roche Complete Protease inhibitor, EDTA-free). CUT&RUN experiments were
822 performed as previously described (Meers et al., 2019) with minor modifications. 0.025%
823 digitonin was used for the Dig-wash buffer formulation. Antibody incubation was
824 performed overnight at 4°C, followed by Protein A-MNase binding for 1 hour at 4°C. Prior
825 to targeted digestion, cell-bead complexes were washed in low-salt rinse buffer (20mM
826 HEPES pH7.5, 0.5mM spermidine, 0.025% digitonin, plus Roche Complete Protease
827 inhibitor, EDTA-free) followed by targeted digestion in ice-cold high-calcium incubation
828 buffer (3.5 mM HEPES pH 7.5, 10 mM $CaCl_2$, 0.025% Digitonin) for 30 minutes at 0°C.
829 Targeted digestion was halted by replacing the incubation buffer with EGTA-STOP buffer
830 (170 mM NaCl, 20 mM EGTA, 0.025% digitonin, 20 µg/ml glycogen, 25 µg/ml RNase A),
831 followed by chromatin release and DNA extraction. Protein AG–MNase was kindly
832 provided by Dr. Steve Henikoff. A rabbit polyclonal Anti-TFAP2E antibody (Proteintech
833 25829-1-AP) was used at a concentration of 1:50 for CUT&RUN experiments.
834
835 ***CUT&RUN library preparation***
836 CUT&RUN libraries were prepared using the NEBNext ultra II DNA library prep kit (New
837 England Biolabs E7645). Quality control of prepared libraries was conducted using an
838 ABI 3730xl DNA analyzer for fragment analysis. Libraries were pooled to equimolar

concentrations and sequenced with paired-end 37-bp reads on an Illumina NextSeq 500 instrument.

QUANTIFICATION AND STATISTICAL ANALYSIS

Quantification and statistical analyses of microscopy data.

All data were collected from mice kept under similar housing conditions in transparent cages on a normal 12 hr. light/dark cycle. Tissue collected from either males or females in the same genotype/treatment group were analyzed together unless otherwise stated. Ages analyzed are indicated in text and figures. The data are presented as mean ± SEM. Prism 9.2.0 was used for statistical analyses, including calculation of mean values, and standard errors. Two-tailed, unpaired t-test were used for all statistical analyses, and calculated p-values <0.05 were considered statistically significant. Sample sizes and p-values are indicated as single points in each graph and/or in figure legends.

Measurements of VNE and cell counts were performed on confocal images or bright field images of coronal serial sections immunostained or in situ hybridizations for the indicated targets. In animals ≥P15, the most central 6-8 sections on the rostro-caudal axis of the VNO were quantified and averaged, and in animals ≥P0, the most medial 4-6 sections were quantified and averaged. Measurements and quantifications were performed using ImageJ 2.1.0 and Imaris. Statistical differences between genotypes were quantified with two-tailed unpaired t-test using Prism 9.2.0, (GraphPad Software, CA, USA). Microscopy data reported in this paper will be shared by the lead contact upon request.

CUT&RUN data analysis

In processing CUT&RUN data, paired-end sequencing reads were trimmed using Cutadapt t(Martin, 2011) using the following arguments: "-a AGATCGGAAGAGCACACGTCTGAACTCCAGTCA -A AGATCGGAAGAGCGTCGTGTAGGGAAAGAGTGT --minimum-length=25". Reads were aligned to the reference mouse mm10 assembly from the UCSC genome browser using Bowtie 2 (Langmead and Salzberg, 2012) using the following arguments: "--local -

870 -very-sensitive-local --no-unal --no-mixed --no-discordant -I 10 -X 1000". BAM files were
871 filtered with SAMtools to discard unmapped reads, those which were not the primary
872 alignment, reads failing platform/vendor quality checks, and PCR/optical duplicates (-f 2
873 -F 780). Peak calling was performed using MACS2 (Zhang et al., 2008). Peak-gene
874 annotation was done by mapping peaks to their closest annotated gene using the
875 ChIPseeker R package(Yu et al., 2015). GO term analysis was performed in R using
876 clusterProfiler (Yu et al., 2012). Motif enrichment analysis was performed using HOMER
877 (Heinz et al., 2010). The data from this CUT&RUN experiment has been deposited into
878 the NCBI's Expression Omnibus and are accessible through GEO series accession
879 number GSE193139
880 (https://www.ncbi.nlm.nih.gov/geo/query/acc.cgi?acc=GSE193139).
881
882
883

884 **REFERENCES**

885

886 Arlotta, P., Molyneaux, B.J., Chen, J., Inoue, J., Kominami, R., and Macklis, J.D. (2005).
887 Neuronal subtype-specific genes that control corticospinal motor neuron development in
888 vivo. Neuron *45*, 207-221.
889 Bahreini Jangjoo, S., Lin, J.M., Etaati, F., Fearnley, S., Cloutier, J.-F., Khmaladze, A., and
890 Forni, P.E. (2021). Automated quantification of vomeronasal glomeruli number, size, and
891 color composition after immunofluorescent staining. Chemical Senses.
892 Bamforth, S.D., Bragança, J., Eloranta, J.J., Murdoch, J.N., Marques, F.I.R., Kranc, K.R.,
893 Farza, H., Henderson, D.J., Hurst, H.C., and Bhattacharya, S. (2001). Cardiac
894 malformations, adrenal agenesis, neural crest defects and exencephaly in mice lacking
895 Cited2, a new Tfap2 co-activator. Nature Genetics *29*, 469-474.
896 Bassett, E.A., Korol, A., Deschamps, P.A., Buettner, R., Wallace, V.A., Williams, T., and
897 West-Mays, J.A. (2012). Overlapping Expression Patterns and Redundant Roles for AP-
898 2 Transcription Factors in the Developing Mammalian Retina. Developmental dynamics :
899 an official publication of the American Association of Anatomists *241*, 814-829.
900 Berghard, A., and Buck, L.B. (1996). Sensory transduction in vomeronasal neurons:
901 evidence for G alpha o, G alpha i2, and adenylyl cyclase II as major components of a
902 pheromone signaling cascade. The Journal of Neuroscience *16*, 909-918.
903 Bragança, J., Eloranta, J.J., Bamforth, S.D., Ibbitt, J.C., Hurst, H.C., and Bhattacharya,
904 S. (2003). Physical and functional interactions among AP-2 transcription factors,
905 p300/CREB-binding protein, and CITED2. J Biol Chem *278*, 16021-16029.
906 Buiakova, O.I., Krishna, N.S., Getchell, T.V., and Margolis, F.L. (1994). Human and
907 rodent OMP genes: conservation of structural and regulatory motifs and cellular
908 localization. Genomics *20*, 452-462.
909 Cau, E., Casarosa, S., and Guillemot, F. (2002). Mash1 and Ngn1 control distinct steps
910 of determination and differentiation in the olfactory sensory neuron lineage. Development
911 *129*, 1871-1880.
912 Cau, E., Gradwohl, G., Fode, C., and Guillemot, F. (1997). Mash1 activates a cascade of
913 bHLH regulators in olfactory neuron progenitors. Development *124*, 1611-1621.
914 Chambers, B.E., Gerlach, G.F., Clark, E.G., Chen, K.H., Levesque, A.E., Leshchiner, I.,
915 Goessling, W., and Wingert, R.A. (2019). Tfap2a is a novel gatekeeper of nephron
916 differentiation during kidney development. Development *146*, dev172387.
917 Chamero, P., Katsoulidou, V., Hendrix, P., Bufe, B., Roberts, R., Matsunami, H.,
918 Abramowitz, J., Birnbaumer, L., Zufall, F., and Leinders-Zufall, T. (2011). G protein
919 G(alpha)o is essential for vomeronasal function and aggressive behavior in mice. Proc
920 Natl Acad Sci U S A *108*, 12898-12903.
921 Chamero, P., Marton, T.F., Logan, D.W., Flanagan, K., Cruz, J.R., Saghatelian, A.,
922 Cravatt, B.F., and Stowers, L. (2007). Identification of protein pheromones that promote
923 aggressive behaviour. Nature *450*, 899-902.
924 Cho, J.H., Prince, J.E., Cutforth, T., and Cloutier, J.F. (2011). The pattern of glomerular
925 map formation defines responsiveness to aversive odorants in mice. J Neurosci *31*, 7920-
926 7926.

927 Cloutier, J.F., Giger, R.J., Koentges, G., Dulac, C., Kolodkin, A.L., and Ginty, D.D. (2002).
928 Neuropilin-2 mediates axonal fasciculation, zonal segregation, but not axonal
929 convergence, of primary accessory olfactory neurons. Neuron *33*, 877-892.
930 de la Rosa-Prieto, C., Saiz-Sanchez, D., Ubeda-Banon, I., Argandona-Palacios, L.,
931 Garcia-Munozguren, S., and Martinez-Marcos, A. (2010). Neurogenesis in subclasses of
932 vomeronasal sensory neurons in adult mice. Dev Neurobiol *70*, 961-970.
933 Dey, S., and Matsunami, H. (2011). Calreticulin chaperones regulate functional
934 expression of vomeronasal type 2 pheromone receptors. Proc Natl Acad Sci U S A *108*,
935 16651-16656.
936 Dudley, C.A., and Moss, R.L. (1999). Activation of an anatomically distinct subpopulation
937 of accessory olfactory bulb neurons by chemosensory stimulation. Neuroscience *91*,
938 1549-1556.
939 Dulac, C., and Axel, R. (1995). A novel family of genes encoding putative pheromone
940 receptors in mammals. Cell *83*, 195-206.
941 Eckert, D., Buhl, S., Weber, S., Jager, R., and Schorle, H. (2005). The AP-2 family of
942 transcription factors. Genome Biol *6*, 246.
943 Enomoto, T., Ohmoto, M., Iwata, T., Uno, A., Saitou, M., Yamaguchi, T., Kominami, R.,
944 Matsumoto, I., and Hirota, J. (2011). Bcl11b/Ctip2 controls the differentiation of
945 vomeronasal sensory neurons in mice. J Neurosci *31*, 10159-10173.
946 Fagotto, F. (2014). The cellular basis of tissue separation. Development *141*, 3303-3318.
947 Farbman, A.I., and Margolis, F.L. (1980). Olfactory marker protein during ontogeny:
948 immunohistochemical localization. Dev Biol *74*, 205-215.
949 Feng, W., Simoes-de-Souza, F., Finger, T.E., Restrepo, D., and Williams, T. (2009).
950 Disorganized olfactory bulb lamination in mice deficient for transcription factor AP-
951 2epsilon. Mol Cell Neurosci *42*, 161-171.
952 Feng, W., and Williams, T. (2003). Cloning and characterization of the mouse AP-2
953 epsilon gene: a novel family member expressed in the developing olfactory bulb. Mol Cell
954 Neurosci *24*, 460-475.
955 Fernandez Garcia, M., Moore, C.D., Schulz, K.N., Alberto, O., Donague, G., Harrison,
956 M.M., Zhu, H., and Zaret, K.S. (2019). Structural Features of Transcription Factors
957 Associating with Nucleosome Binding. Mol Cell *75*, 921-932 e926.
958 Forni, P.E., Fornaro, M., Guenette, S., and Wray, S. (2011). A role for FE65 in controlling
959 GnRH-1 neurogenesis. J Neurosci *31*, 480-491.
960 Heinz, S., Benner, C., Spann, N., Bertolino, E., Lin, Y.C., Laslo, P., Cheng, J.X., Murre,
961 C., Singh, H., and Glass, C.K. (2010). Simple combinations of lineage-determining
962 transcription factors prime cis-regulatory elements required for macrophage and B cell
963 identities. Mol Cell *38*, 576-589.
964 Herrada, G., and Dulac, C. (1997). A novel family of putative pheromone receptors in
965 mammals with a topographically organized and sexually dimorphic distribution. Cell *90*,
966 763-773.
967 Hobert, O. (2008). Regulatory logic of neuronal diversity: terminal selector genes and
968 selector motifs. Proc Natl Acad Sci U S A *105*, 20067-20071.
969 Hobert, O., and Kratsios, P. (2019). Neuronal identity control by terminal selectors in
970 worms, flies, and chordates. Curr Opin Neurobiol *56*, 97-105.
971 Huang, Y.H., Jankowski, A., Cheah, K.S., Prabhakar, S., and Jauch, R. (2015). SOXE
972 transcription factors form selective dimers on non-compact DNA motifs through

973 multifaceted interactions between dimerization and high-mobility group domains. Sci Rep
974 *5*, 10398.
975 Isogai, Y., Si, S., Pont-Lezica, L., Tan, T., Kapoor, V., Murthy, V.N., and Dulac, C. (2011).
976 Molecular organization of vomeronasal chemoreception. Nature *478*, 241-245.
977 Jia, C., and Halpern, M. (1996). Subclasses of vomeronasal receptor neurons: differential
978 expression of G proteins (Gi alpha 2 and G(o alpha)) and segregated projections to the
979 accessory olfactory bulb. Brain Res *719*, 117-128.
980 Kantarci, H., Edlund, R.K., Groves, A.K., and Riley, B.B. (2015). Tfap2a Promotes
981 Specification and Maturation of Neurons in the Inner Ear through Modulation of Bmp, Fgf
982 and Notch Signaling. PLoS Genetics *11*, e1005037.
983 Katreddi, R.R., and Forni, P.E. (2021). Mechanisms underlying pre- and postnatal
984 development of the vomeronasal organ. Cell Mol Life Sci.
985 Katreddi, R.R., Taroc, E.Z.M., Hicks, S.M., Lin, J.M., Liu, S., Xiang, M., and Forni, P.E.
986 (2022). Notch signaling determines cell-fate specification of the two main types of
987 vomeronasal neurons of rodents. Development *149*.
988 Keller, M., Pierman, S., Douhard, Q., Baum, M.J., and Bakker, J. (2006). The
989 vomeronasal organ is required for the expression of lordosis behaviour, but not sex
990 discrimination in female mice. Eur J Neurosci *23*, 521-530.
991 Kimoto, H., Haga, S., Sato, K., and Touhara, K. (2005). Sex-specific peptides from
992 exocrine glands stimulate mouse vomeronasal sensory neurons. Nature *437*, 898-901.
993 Koolhaas, J.M., Coppens, C.M., de Boer, S.F., Buwalda, B., Meerlo, P., and
994 Timmermans, P.J.A. (2013). The resident-intruder paradigm: a standardized test for
995 aggression, violence and social stress. Journal of visualized experiments : JoVE, e4367-
996 e4367.
997 Krieger, J., Schmitt, A., Lobel, D., Gudermann, T., Schultz, G., Breer, H., and Boekhoff,
998 I. (1999). Selective activation of G protein subtypes in the vomeronasal organ upon
999 stimulation with urine-derived compounds. J Biol Chem *274*, 4655-4662.
1000 Langmead, B., and Salzberg, S.L. (2012). Fast gapped-read alignment with Bowtie 2. Nat
1001 Methods *9*, 357-359.
1002 Lin, J.M., Taroc, E.Z.M., Frias, J.A., Prasad, A., Catizone, A.N., Sammons, M.A., and
1003 Forni, P.E. (2018). The transcription factor Tfap2e/AP-2epsilon plays a pivotal role in
1004 maintaining the identity of basal vomeronasal sensory neurons. Dev Biol *441*, 67-82.
1005 Luo, L., Ambrozkiewicz, M.C., Benseler, F., Chen, C., Dumontier, E., Falkner, S.,
1006 Furlanis, E., Gomez, A.M., Hoshina, N., Huang, W.H.*, et al.* (2020). Optimizing Nervous
1007 System-Specific Gene Targeting with Cre Driver Lines: Prevalence of Germline
1008 Recombination and Influencing Factors. Neuron *106*, 37-65 e35.
1009 Lupien, M., Eeckhoute, J., Meyer, C.A., Wang, Q., Zhang, Y., Li, W., Carroll, J.S., Liu,
1010 X.S., and Brown, M. (2008). FoxA1 translates epigenetic signatures into enhancer-driven
1011 lineage-specific transcription. Cell *132*, 958-970.
1012 Magnani, L., Eeckhoute, J., and Lupien, M. (2011). Pioneer factors: directing
1013 transcriptional regulators within the chromatin environment. Trends Genet *27*, 465-474.
1014 Mangale, V.S., Hirokawa, K.E., Satyaki, P.R., Gokulchandran, N., Chikbire, S.,
1015 Subramanian, L., Shetty, A.S., Martynoga, B., Paul, J., Mai, M.V.*, et al.* (2008). Lhx2
1016 selector activity specifies cortical identity and suppresses hippocampal organizer fate.
1017 Science *319*, 304-309.

1018 Martin, M. (2011). Cutadapt removes adapter sequences from high-throughput
1019 sequencing reads. EMBnetjournal *17*, 10-12.
1020 Martinez-Marcos, A., Ubeda-Banon, I., and Halpern, M. (2000). Cell turnover in the
1021 vomeronasal epithelium: evidence for differential migration and maturation of subclasses
1022 of vomeronasal neurons in the adult opossum. J Neurobiol *43*, 50-63.
1023 Matsunami, H., and Buck, L.B. (1997). A multigene family encoding a diverse array of
1024 putative pheromone receptors in mammals. Cell *90*, 775-784.
1025 Meers, M.P., Bryson, T.D., Henikoff, J.G., and Henikoff, S. (2019). Improved CUT&RUN
1026 chromatin profiling tools. Elife *8*.
1027 Mohrhardt, J., Nagel, M., Fleck, D., Ben-Shaul, Y., and Spehr, M. (2018). Signal Detection
1028 and Coding in the Accessory Olfactory System. Chemical Senses *43*, 667-695.
1029 Molyneaux, B.J., Arlotta, P., Menezes, J.R., and Macklis, J.D. (2007). Neuronal subtype
1030 specification in the cerebral cortex. Nat Rev Neurosci *8*, 427-437.
1031 Mombaerts, P., Wang, F., Dulac, C., Chao, S.K., Nemes, A., Mendelsohn, M.,
1032 Edmondson, J., and Axel, R. (1996). Visualizing an olfactory sensory map. Cell *87*, 675-
1033 686.
1034 Monahan, K., Schieren, I., Cheung, J., Mumbey-Wafula, A., Monuki, E.S., and
1035 Lomvardas, S. (2017). Cooperative interactions enable singular olfactory receptor
1036 expression in mouse olfactory neurons. Elife *6*.
1037 Montani, G., Tonelli, S., Sanghez, V., Ferrari, P.F., Palanza, P., Zimmer, A., and Tirindelli,
1038 R. (2013). Aggressive behaviour and physiological responses to pheromones are strongly
1039 impaired in mice deficient for the olfactory G-protein -subunit G8. J Physiol *591*, 3949-
1040 3962.
1041 Murray, R.C., Navi, D., Fesenko, J., Lander, A.D., and Calof, A.L. (2003). Widespread
1042 defects in the primary olfactory pathway caused by loss of Mash1 function. J Neurosci
1043 *23*, 1769-1780.
1044 Naik, A.S., Lin, J.M., Taroc, E.Z.M., Katreddi, R.R., Frias, J.A., Lemus, A.A., Sammons,
1045 M.A., and Forni, P.E. (2020). Smad4-dependent morphogenic signals control the
1046 maturation and axonal targeting of basal vomeronasal sensory neurons to the accessory
1047 olfactory bulb. Development *147*, dev184036.
1048 Norlin, E.M., Alenius, M., Gussing, F., Hagglund, M., Vedin, V., and Bohm, S. (2001).
1049 Evidence for gradients of gene expression correlating with zonal topography of the
1050 olfactory sensory map. Mol Cell Neurosci *18*, 283-295.
1051 Oboti, L., Ibarra-Soria, X., Perez-Gomez, A., Schmid, A., Pyrski, M., Paschek, N., Kircher,
1052 S., Logan, D.W., Leinders-Zufall, T., Zufall, F.*, et al.* (2015). Pregnancy and estrogen
1053 enhance neural progenitor-cell proliferation in the vomeronasal sensory epithelium. BMC
1054 Biol *13*, 104.
1055 Oboti, L., Perez-Gomez, A., Keller, M., Jacobi, E., Birnbaumer, L., Leinders-Zufall, T.,
1056 Zufall, F., and Chamero, P. (2014). A wide range of pheromone-stimulated sexual and
1057 reproductive behaviors in female mice depend on G protein Galphao. BMC Biol *12*, 31.
1058 Pankevich, D.E., Baum, M.J., and Cherry, J.A. (2004). Olfactory sex discrimination
1059 persists, whereas the preference for urinary odorants from estrous females disappears in
1060 male mice after vomeronasal organ removal. J Neurosci *24*, 9451-9457.
1061 Patel, T., and Hobert, O. (2017). Coordinated control of terminal differentiation and
1062 restriction of cellular plasticity. Elife *6*.

1063 Patel, T., Tursun, B., Rahe, D.P., and Hobert, O. (2012). Removal of Polycomb repressive
1064 complex 2 makes C. elegans germ cells susceptible to direct conversion into specific
1065 somatic cell types. Cell Rep *2*, 1178-1186.
1066 Pellikainen, J.M., and Kosma, V.M. (2007). Activator protein-2 in carcinogenesis with a
1067 special reference to breast cancer--a mini review. Int J Cancer *120*, 2061-2067.
1068 Pereira, L., Aeschimann, F., Wang, C., Lawson, H., Serrano-Saiz, E., Portman, D.S.,
1069 Grosshans, H., and Hobert, O. (2019). Timing mechanism of sexually dimorphic nervous
1070 system differentiation. Elife *8*.
1071 Perez-Gomez, A., Stein, B., Leinders-Zufall, T., and Chamero, P. (2014). Signaling
1072 mechanisms and behavioral function of the mouse basal vomeronasal neuroepithelium.
1073 Front Neuroanat *8*, 135.
1074 Polanco, J., Reyes-Vigil, F., Weisberg, S.D., Dhimitruka, I., and Bruses, J.L. (2021).
1075 Differential Spatiotemporal Expression of Type I and Type II Cadherins Associated With
1076 the Segmentation of the Central Nervous System and Formation of Brain Nuclei in the
1077 Developing Mouse. Front Mol Neurosci *14*, 633719.
1078 Prince, J.E., Brignall, A.C., Cutforth, T., Shen, K., and Cloutier, J.F. (2013). Kirrel3 is
1079 required for the coalescence of vomeronasal sensory neuron axons into glomeruli and for
1080 male-male aggression. Development *140*, 2398-2408.
1081 Prince, J.E., Cho, J.H., Dumontier, E., Andrews, W., Cutforth, T., Tessier-Lavigne, M.,
1082 Parnavelas, J., and Cloutier, J.F. (2009). Robo-2 controls the segregation of a portion of
1083 basal vomeronasal sensory neuron axons to the posterior region of the accessory
1084 olfactory bulb. J Neurosci *29*, 14211-14222.
1085 Rahe, D.P., and Hobert, O. (2019). Restriction of Cellular Plasticity of Differentiated Cells
1086 Mediated by Chromatin Modifiers, Transcription Factors and Protein Kinases. G3
1087 (Bethesda) *9*, 2287-2302.
1088 Rothstein, M., and Simoes-Costa, M. (2020). Heterodimerization of TFAP2 pioneer
1089 factors drives epigenomic remodeling during neural crest specification. Genome Res *30*,
1090 35-48.
1091 Ryba, N.J., and Tirindelli, R. (1997). A new multigene family of putative pheromone
1092 receptors. Neuron *19*, 371-379.
1093 Seberg, H.E., Van Otterloo, E., Loftus, S.K., Liu, H., Bonde, G., Sompallae, R., Gildea,
1094 D.E., Santana, J.F., Manak, J.R., Pavan, W.J.*, et al.* (2017). TFAP2 paralogs regulate
1095 melanocyte differentiation in parallel with MITF. PLoS Genet *13*, e1006636.
1096 Silva, L., and Antunes, A. (2017). Vomeronasal Receptors in Vertebrates and the
1097 Evolution of Pheromone Detection. Annu Rev Anim Biosci *5*, 353-370.
1098 Silvotti, L., Cavalca, E., Gatti, R., Percudani, R., and Tirindelli, R. (2011). A recent class
1099 of chemosensory neurons developed in mouse and rat. PLoS One *6*, e24462.
1100 Silvotti, L., Cavaliere, R.M., Belletti, S., and Tirindelli, R. (2018). In-vivo activation of
1101 vomeronasal neurons shows adaptive responses to pheromonal stimuli. Sci Rep *8*, 8490.
1102 Skene, P.J., Henikoff, J.G., and Henikoff, S. (2018). Targeted in situ genome-wide
1103 profiling with high efficiency for low cell numbers. Nat Protoc *13*, 1006-1019.
1104 Skene, P.J., and Henikoff, S. (2017). An efficient targeted nuclease strategy for high-
1105 resolution mapping of DNA binding sites. Elife *6*.
1106 Stefanakis, N., Carrera, I., and Hobert, O. (2015). Regulatory Logic of Pan-Neuronal
1107 Gene Expression in C. elegans. Neuron *87*, 733-750.

1108 Stowers, L., Holy, T.E., Meister, M., Dulac, C., and Koentges, G. (2002). Loss of sex
1109 discrimination and male-male aggression in mice deficient for TRP2. Science *295*, 1493-
1110 1500.
1111 Taroc, E.Z.M., Naik, A.S., Lin, J.M., Peterson, N.B., Keefe, D.L., Jr., Genis, E., Fuchs, G.,
1112 Balasubramanian, R., and Forni, P.E. (2020). Gli3 Regulates Vomeronasal
1113 Neurogenesis, Olfactory Ensheathing Cell Formation, and GnRH-1 Neuronal Migration.
1114 J Neurosci *40*, 311-326.
1115 Trouillet, A.C., Keller, M., Weiss, J., Leinders-Zufall, T., Birnbaumer, L., Zufall, F., and
1116 Chamero, P. (2019). Central role of G protein Galphai2 and Galphai2(+) vomeronasal
1117 neurons in balancing territorial and infant-directed aggression of male mice. Proc Natl
1118 Acad Sci U S A *116*, 5135-5143.
1119 Trouillet, A.C., Moussu, C., Poissenot, K., Keller, M., Birnbaumer, L., Leinders-Zufall, T.,
1120 Zufall, F., and Chamero, P. (2021). Sensory Detection by the Vomeronasal Organ
1121 Modulates Experience-Dependent Social Behaviors in Female Mice. Front Cell Neurosci
1122 *15*, 638800.
1123 Vaddadi, N., Iversen, K., Raja, R., Phen, A., Brignall, A., Dumontier, E., and Cloutier, J.F.
1124 (2019). Kirrel2 is differentially required in populations of olfactory sensory neurons for the
1125 targeting of axons in the olfactory bulb. Development *146*.
1126 Walz, A., Rodriguez, I., and Mombaerts, P. (2002). Aberrant sensory innervation of the
1127 olfactory bulb in neuropilin-2 mutant mice. J Neurosci *22*, 4025-4035.
1128 Wankhade, S., Yu, Y., Weinberg, J., Tainsky, M.A., and Kannan, P. (2000).
1129 Characterization of the activation domains of AP-2 family transcription factors. J Biol
1130 Chem *275*, 29701-29708.
1131 Weiler, E., McCulloch, M.A., and Farbman, A.I. (1999). Proliferation in the vomeronasal
1132 organ of the rat during postnatal development. Eur J Neurosci *11*, 700-711.
1133 Williams, C.M., Scibetta, A.G., Friedrich, J.K., Canosa, M., Berlato, C., Moss, C.H., and
1134 Hurst, H.C. (2009). AP-2gamma promotes proliferation in breast tumour cells by direct
1135 repression of the CDKN1A gene. EMBO J *28*, 3591-3601.
1136 Wilson, K.C.P., and Raisman, G. (1980). Age-related changes in the neurosensory
1137 epithelium of the mouse vomeronasal organ: Extended period of post-natal growth in size
1138 and evidence for rapid cell turnover in the adult. Brain Research *185*, 103-113.
1139 Yu, G., Wang, L.G., Han, Y., and He, Q.Y. (2012). clusterProfiler: an R package for
1140 comparing biological themes among gene clusters. OMICS *16*, 284-287.
1141 Yu, G., Wang, L.G., and He, Q.Y. (2015). ChIPseeker: an R/Bioconductor package for
1142 ChIP peak annotation, comparison and visualization. Bioinformatics *31*, 2382-2383.
1143 Zhang, Y., Liu, T., Meyer, C.A., Eeckhoute, J., Johnson, D.S., Bernstein, B.E., Nusbaum,
1144 C., Myers, R.M., Brown, M., Li, W.*, et al.* (2008). Model-based analysis of ChIP-Seq
1145 (MACS). Genome Biol *9*, R137.
1146 Zuloaga, D.G., Morris, J.A., Monks, D.A., Breedlove, S.M., and Jordan, C.L. (2007).
1147 Androgen-sensitivity of somata and dendrites of spinal nucleus of the bulbocavernosus
1148 (SNB) motoneurons in male C57BL6J mice. Horm Behav *51*, 207-212.
1149

1150

1151 **GRAPHICAL ABSTRACT**

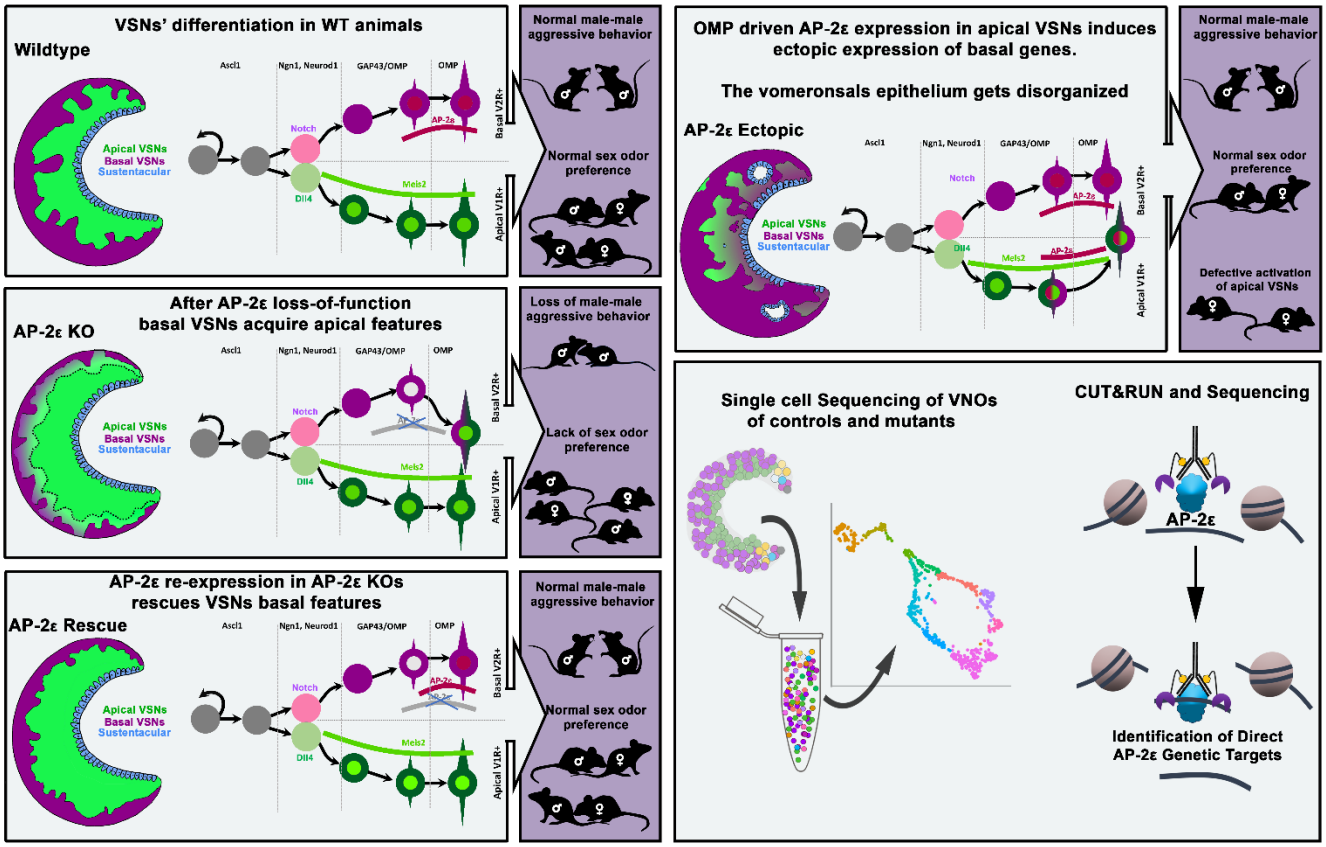

1152
1153

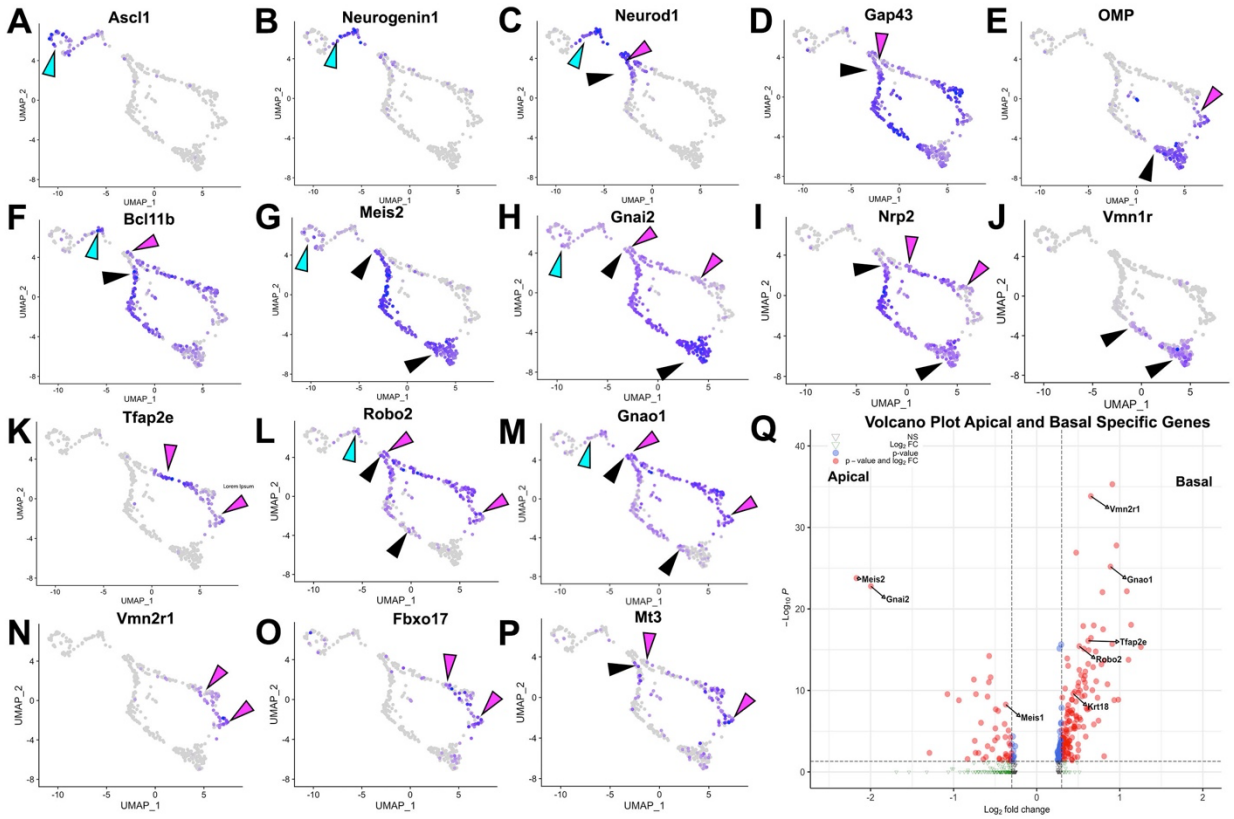

Figure 1: Analysis of single cell sequencing data of the vomeronasal organ. P10 male controls shows the developing vomeronasal neurons as they progress through A-C) neurogenesis (Ascl1, Neurog1, Neurod1), D-F) maturation (Gap43, OMP, Bcl11b), G-J) apical VSNs' differentiation/maturation (Meis2, Gnai2, Nrp2, Vmn1r) and K-P) basal VSNs' differentiation/maturation (Tfap2e, Robo2, Gnao1, Vmn2r1, Fbxo17, Mt3). A) Ascl1 is expressed by transiently amplifying progenitor cells (cyan arrow), which transition into the immediate neuronal precursors that turn on pro-neural genes (cyan arrow) Neurog1 (B) and Neurod1 (C) and turn off as the precursors turn into immature neurons (black and magenta). D) Immature neurons express Gap43, which persists in both apical (black arrow) and basal (magenta arrow) branches, until it declines as neurons begin to reach maturity and express E) OMP in mature apical (black arrow) and mature basal (magenta arrow) VSNs. Gap43 and OMP expression briefly overlap, as the neurons transition to a fully differentiated mature stage. F) Bcl11b mRNA expression is found in both apical and basal VSNs but at different developmental timepoints. Bcl11b is found in committed basal precursors near the establishment of the apical/basal dichotomy (magenta arrow) but is not found until later in apical VSN development (black arrow) G) Meis2 mRNA expression is found in the apical branch (black arrows) and even in early neurogenesis stages (cyan arrow), and their expression does not overlap. H) Gnai2 expression starts in immature apical and basal VSNs. However, its expression increases in mature apical VSNs but fades in mature basal VSNs. I) Nrp2 expression is only retained in mature apical VSNs. J) Vmn1r is only expressed in maturing/mature apical VSNs. K) AP-2ε is expressed by the basal branch (magenta arrows). L) Robo2 expression is only retained in mature basal VSNs. M) Gnao1 expression starts in immature apical and basal VSNs. However, its expression increases in mature basal VSNs but fades in mature apical VSNs. N) Vmn2r1 is restricted to maturing/mature basal VSNs. O) Fbxo17 is mainly expressed in mature/maturing basal VSNs. P) Mt3 is mainly expressed in mature/maturing basal VSNs. Q) Enhanced volcano plot. Differential gene expression between apical and basal branches of VSNs. Apical specific genes (55 genes) trend left and basal specific genes (187 genes) trend right. Significance defined as Log_2-Fold Change > 0.3 and Adjusted p-value ≤ 0.05.

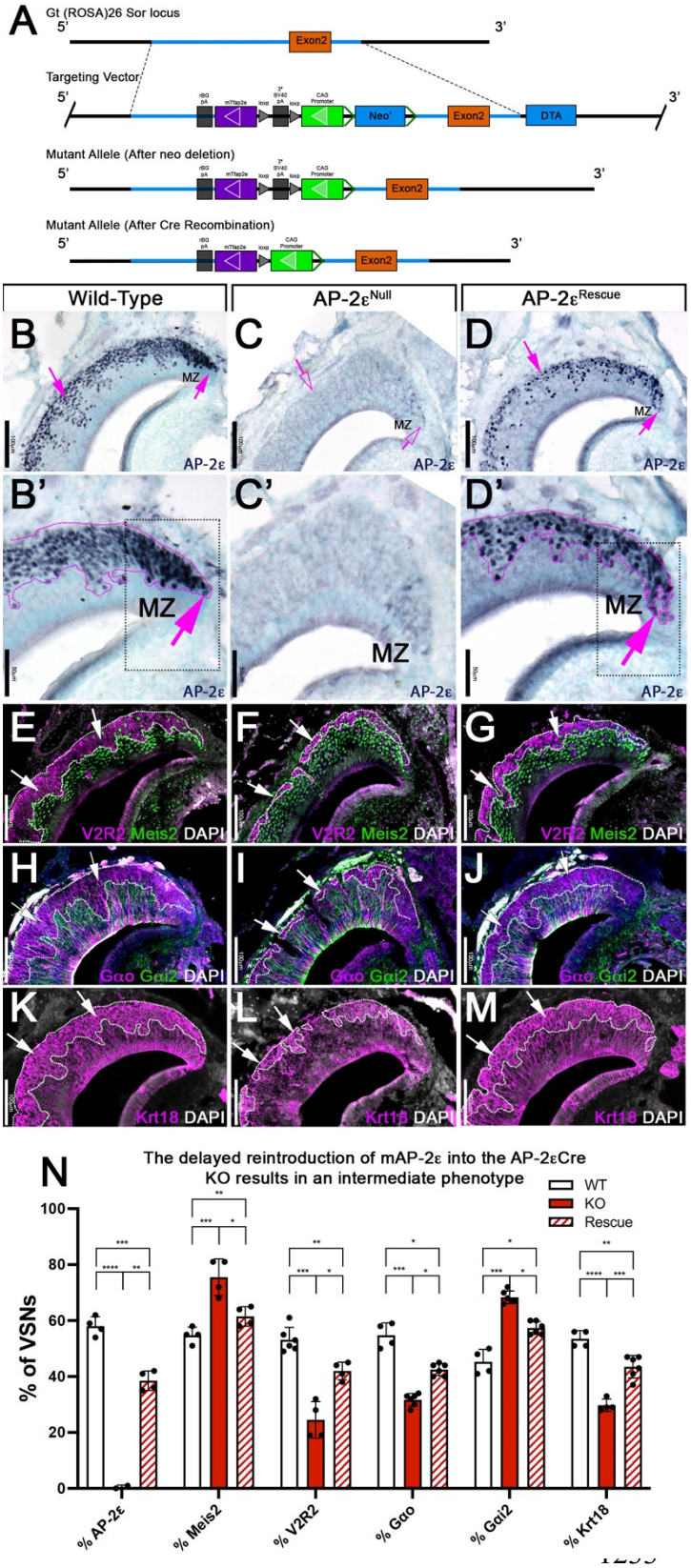

Figure 2: R26AP2ε mouse line **mouse generation and characterization of rescued AP-2ε expression in AP-2ε^{Null} mice.** A) Knock-in strategy through homologous recombination to generate the R26AP2ε mouse line. The CAG-loxP-stop-loxP-mouse-Tfap2e cassette as integrated into the first intron of Rosa26. B-D') Immunohistochemistry on P21 wild-type (B, B'), AP-2ε^{Null} (C,C'), and AP-2ε^{Rescue} (D,D') mice against AP-2ε. B,B') In WT mice AP-2ε expression is in the marginal zones (MZ) and in the basal regions of the VSNs. C,C') In AP-2ε^{Null} mice, some AP-2ε immunoreactivity is observed in the MZ but lost in the central regions where more mature neurons reside. D,D') In the AP-2ε^{Rescue}, AP-2ε is expressed in the basal region, but with less intensity and density at the MZ and in central regions compared to WT controls. E-G) Immunostainings against V2R2 (magenta) and Meis2 (green) counterstained with DAPI (white). H-J) Immunostainings against Gαo (magenta) and Gαi2 (green) counterstained with DAPI). K-M) Immunostainings against Krt18 (magenta) counterstained with DAPI (white). N) Quantifications of the percentage of VSNs expressing apical/basal markers in WT, AP-2ε^{Null} and AP-2ε^{Rescue} mice. AP-2ε^{Null} mice show a dramatic reduction in basal VSNs and apical VSNs occupy most of the epithelium. The AP-2ε^{Rescue} has an intermediate phenotype between WT and AP-2ε^{Null} mice, where the VNE contains more basal VSNs than in the AP-2ε^{Null} mice but does not reach the equivalency of the WT ($p<0.05$=*, $p<0.01$=**, $p<0.001$=***, $p<0.0001$=****). N=4 for WT in % AP-2ε, % meis2, % Gαo, % Gαi2, and % Krt18. N=6 for WT in % V2R2. N=2 for AP-2ε^{Null} in % AP-2ε. N=4 for AP-2ε^{Null} in % Meis2, % V2R2 and % Krt18. N=6 for AP-2ε^{Null} in % Gαo and % Gαi2. N=4 for AP-2ε^{Rescue} in % AP-2ε, % Meis2 and % V2R2. N=6 for AP-2ε^{Rescue} in % Gαo, % Gαi2, and % Krt18.

1234

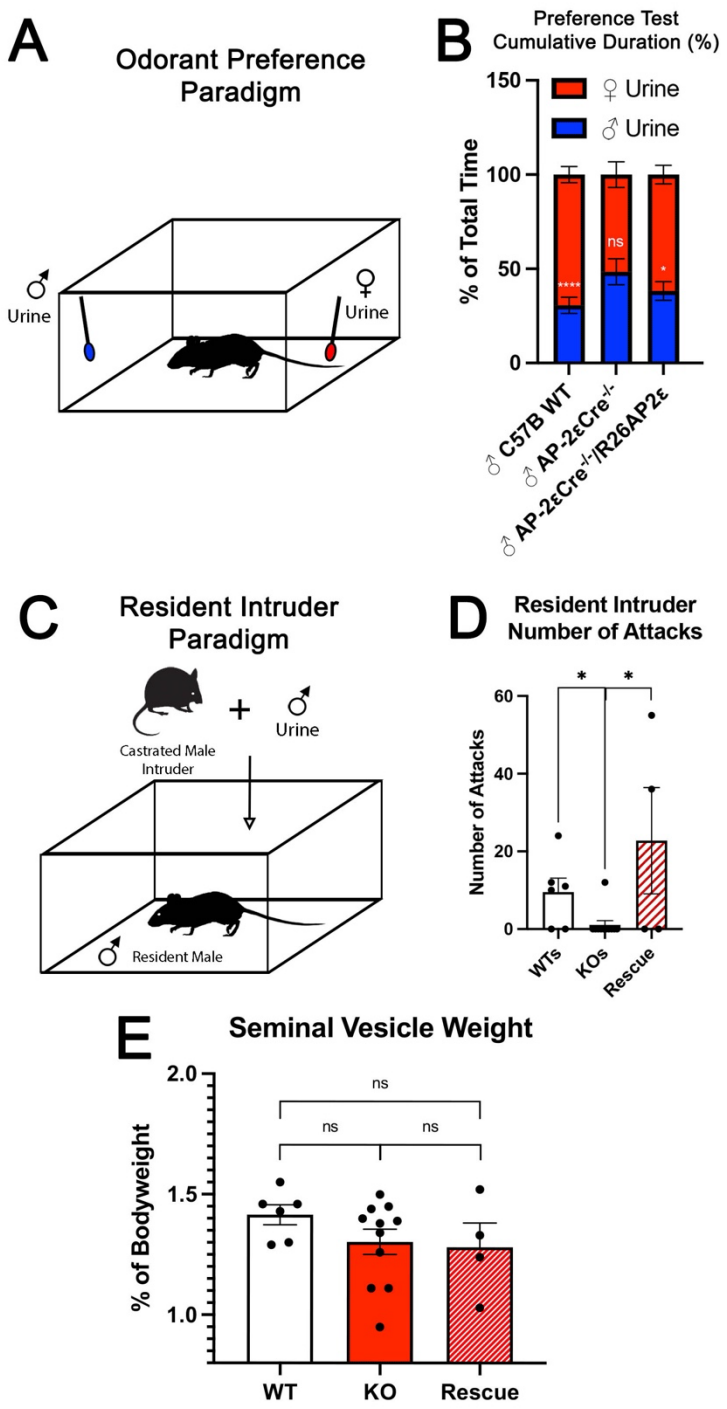

Figure 3: Territorial aggression and sex preference depends on AP-2ε expression in mice. A) The odorant preference paradigm where cotton swabs with either male or female whole urine are placed on opposite ends of a test cage and the amount of time spent smelling each odorant is measured. B) Male WT mice spent significantly more time investigating female odorants than male odorants. Preference for female odorants is lost in AP-2ε KO male mice but restored in AP-2ε rescue mice. ($p<0.05$=*, $p<0.01$=**, $p<0.001$=***). N=6 for WT, n=11 for AP-2ε^{Null} and n=4 for AP-2ε^{Rescue}. C) Male-male aggression was evaluated using the Resident intruder paradigm D) WT mice display aggressive behaviors toward male intruders and number of attacks were quantified. AP-2ε Null mice attacked intruders significantly less than WT mice. However, AP-2ε Rescue mice showed significantly more aggressive behaviors that is not significantly different than the WT male mice. ($p<0.05$=*). N=6 for WT, n=11 for KO, n=4 for rescue. E) Seminal vesicle weight was not significantly different across all genotypes when normalized to bodyweight. N=6 for WT, n=11 for KO, n=4 for rescue.

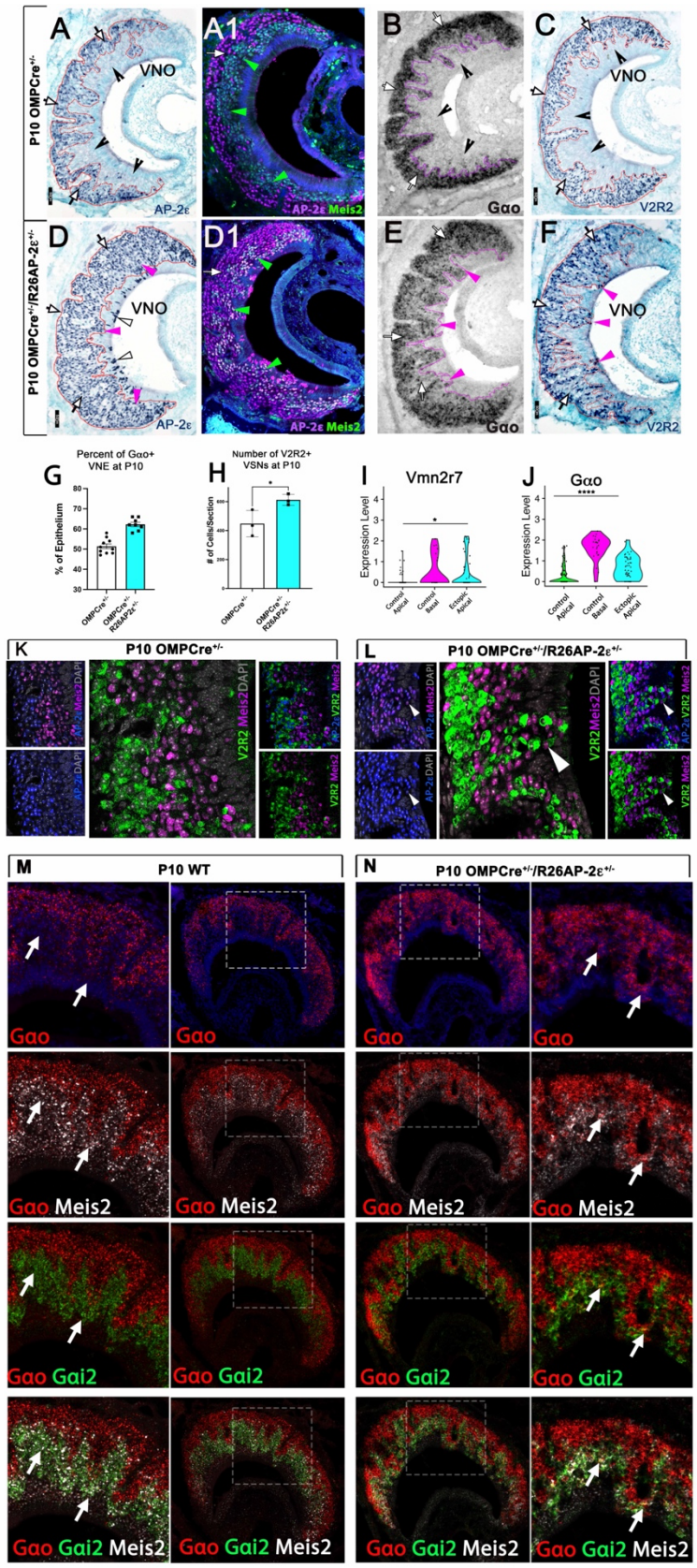
A
A1
B
C
D
D1
E
F
P10 OMPCre+/-
P10 OMPCre+/-/R26AP-2ε+/-
VNO
AP-2ε
AP-2ε Meis2
Gαo
V2R2
G
Percent of Gαo+ VNE at P10
% of Epithelium
H
Number of V2R2+ VSNs at P10
# of Cells/Section
I
Vmn2r7
Expression Level
J
Gαo
K
P10 OMPCre+/-
L
P10 OMPCre+/-/R26AP-2ε+/-
M
P10 WT
N
P10 OMPCre+/-/R26AP-2ε+/-
Gαo
Gαo Meis2
Gαo Gai2
Gαo Gai2 Meis2

1268

<u>Figure 4</u>: Ectopic expression of AP-2ε in the MOE and the VNE promotes expression of basal markers. Immunostainings at P10 on OMPCre$^{+/-}$ controls (A-C) and OMPCre$^{+/-}$/R26AP2ε$^{+/-}$ mutants (D-F). A) IHC against AP-2ε in the VNOs of shows that AP-2ε is expressed in only the basal VSNs (arrow) in controls but have extended AP-2ε immunoreactivity into apical (magenta arrowheads) and sustentacular regions (white arrowheads) in ectopic mutants (D). A1) AP-2ε, Meis2 double immunofluorescence shows segregated AP-2ε (white arrow) and Meis2 (green arrowheads) in controls. D1) In the ectopic mutants AP-2ε expression is detected in Meis2+ cells (green arrowheads). B,E) ISH against Gαo show that in controls (B) Gαo mRNA expression is restricted to the basal regions of the VNE. E) Ectopic AP-2ε mutants show Gαo mRNA reactivity in the apical regions of the VNE (magenta arrowheads). C,F) Immunohistochemistry against V2R2 in the VNO of controls (C) shows no immunoreactivity in the apical regions of the VNE in controls (notched arrows) and is limited to the basal VSNs (white arrows). F) In mutants, more of the vomeronasal epithelium was positive for V2R2 in mutants, as expression expands into the apical regions of the epithelium (magenta arrowheads). G) Quantifications at P10 show an increase in the amount of the neuroepithelium positive for Gαo in OMPCre$^{+/-}$/R26AP-2ε$^{+/-}$ mutants. N=10 for OMPCre$^{+/-}$ controls and n=8 for OMPCre$^{+/-}$/R26AP-2ε$^{+/-}$ mutants. H) Quantifications at P10 show a significant increase in the number of the VSNs positive for V2R2 in OMPCre$^{+/-}$/R26AP-2ε$^{+/-}$ mutants. N=3 for both OMPCre$^{+/-}$ controls and OMPCre$^{+/-}$/R26AP-2ε$^{+/-}$ mutants ($p<0.05$ = *). I,J) Violin plot of Vmn2r7 (I), and Gαo (J) mRNA expression between apical and basal VSNs in OMPCre$^{+/-}$ controls and apical VSNs of OMPCre$^{+/-}$/R26AP2ε$^{+/-}$ mutant mice show significant upregulation of these basal markers in mutants based on p value ($p<0.05$ = *, $p<0.0004$ = ****). K,L) K) Immunofluorescence against V2R2 (magenta) and Meis2 (green) in controls (K) and OMPCre$^{+/-}$/R26AP2ε$^{+/-}$ mutants (L). Arrows indicate a Meis2+ cell immunoreactive against anti V2R2 antibodies in mutants (L). M,N) Single-molecule FISH (RNAscope) against Gαo, Gαi2 and Meis2 of P10 WT and OMPCre$^{+/-}$/R26AP2ε$^{+/-}$ mutants. In WTs (M), a clear segregation between the Gao + (red) basal VSNs and the apical cells positive for Meis2+ (white) and Gai2+ (green) could be seen. In OMPCre$^{+/-}$/R26AP2ε$^{+/-}$ mutants (N) low but obvious expansion of Gao (red) expression to the apical domains of the VNO. Signal highlighting Gao expression could be found in Meis2+ (white) and Gai2+ (green) cells.

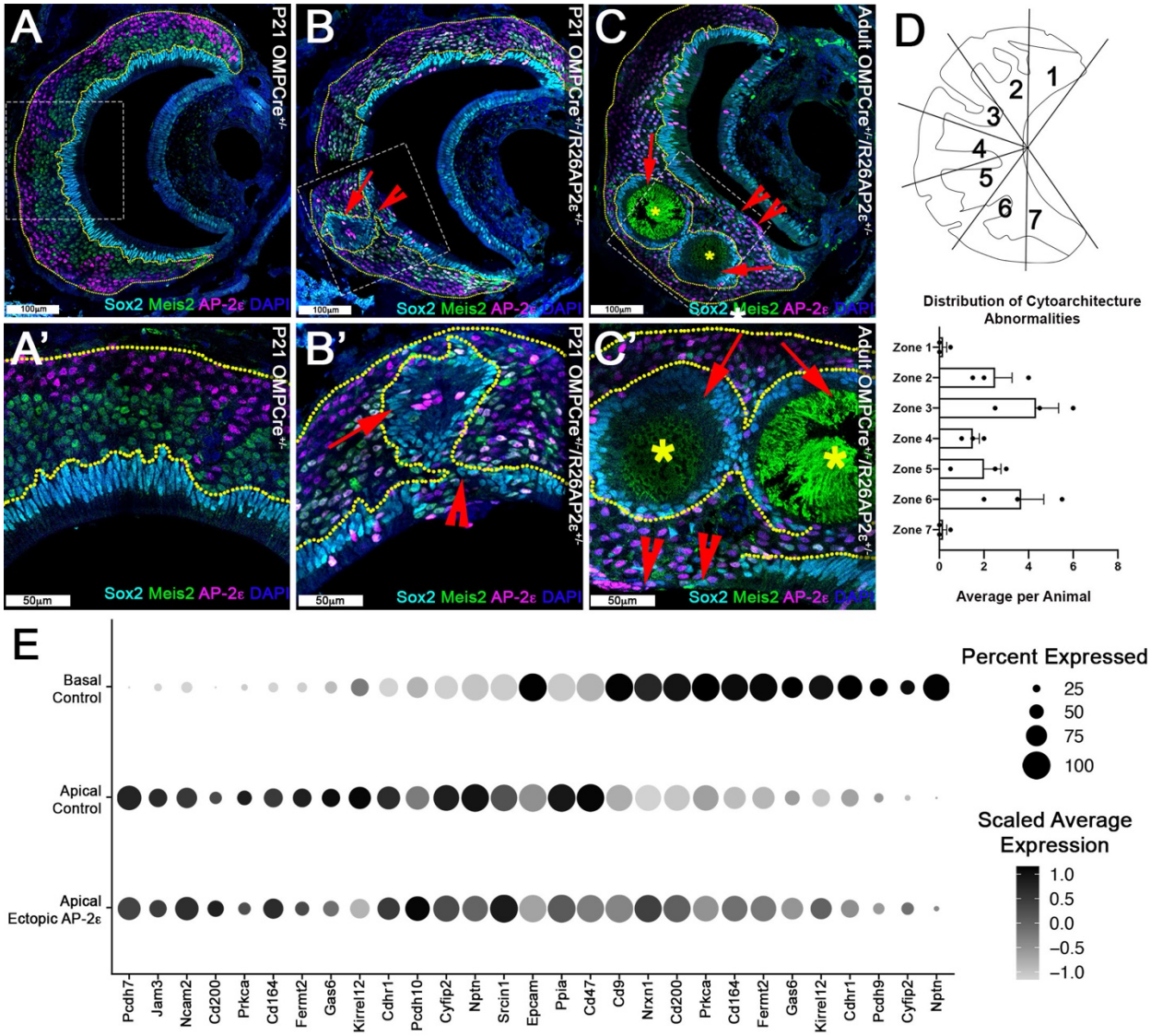

<u>Figure 5:</u> Progressive changes in VNE lamination may reflect the changing expression profiles of cell adhesion molecules in apical VSNs. Immunofluorescence against Sox2 (cyan), AP-2ε (magenta), and Meis2 (green) with DAPI (blue) counterstain. Neuroepithelium traced in yellow dotted line. A) P21 OMPCre$^{+/-}$ controls show highly organized stratified neuroepithelium with contiguous layers of AP-2ε+/basal (magenta), Meis2+/apical (green), and Sox2+/sustentacular cell (cyan) layers. B-C') OMPCre$^{+/-}$/R26AP2ε$^{+/-}$ VNO at B) P21 show that Sox2+/sustentacular cells have intraepithelial cysts with internalized subsidiary lumens (red arrows). C) Adult (3mo) OMPCre$^{+/-}$/R26AP2ε$^{+/-}$ mutants show an increase in the severity of intraepithelial cysts (red arrows) and breaks in the sustentacular layer and expansion of neurons to the luminal surface (red notched arrows). Unidentified matter (*) reactive to anti-mouse Abs was detected within the cysts. D) Quantifications of the zonal distribution through Zone 1 (dorsal) -> Zone 7 (ventral) of these cytoarchitecture abnormalities (which include both cell body abnormalities and dendritic disorganization, each point = 1 animal) show that these disruptions occur in the intermediate and central regions of the VNO, but not in the marginal zones (Zones 1,7). The highest rate of occurrence are in zone 3 and 6, which are intermediate regions in the VNO. N=21 E) Dot plot showing the composition and intensity of differentially expressed genes involved in cellular adhesion in the VSNs of controls and ectopic AP-2ε mutants.

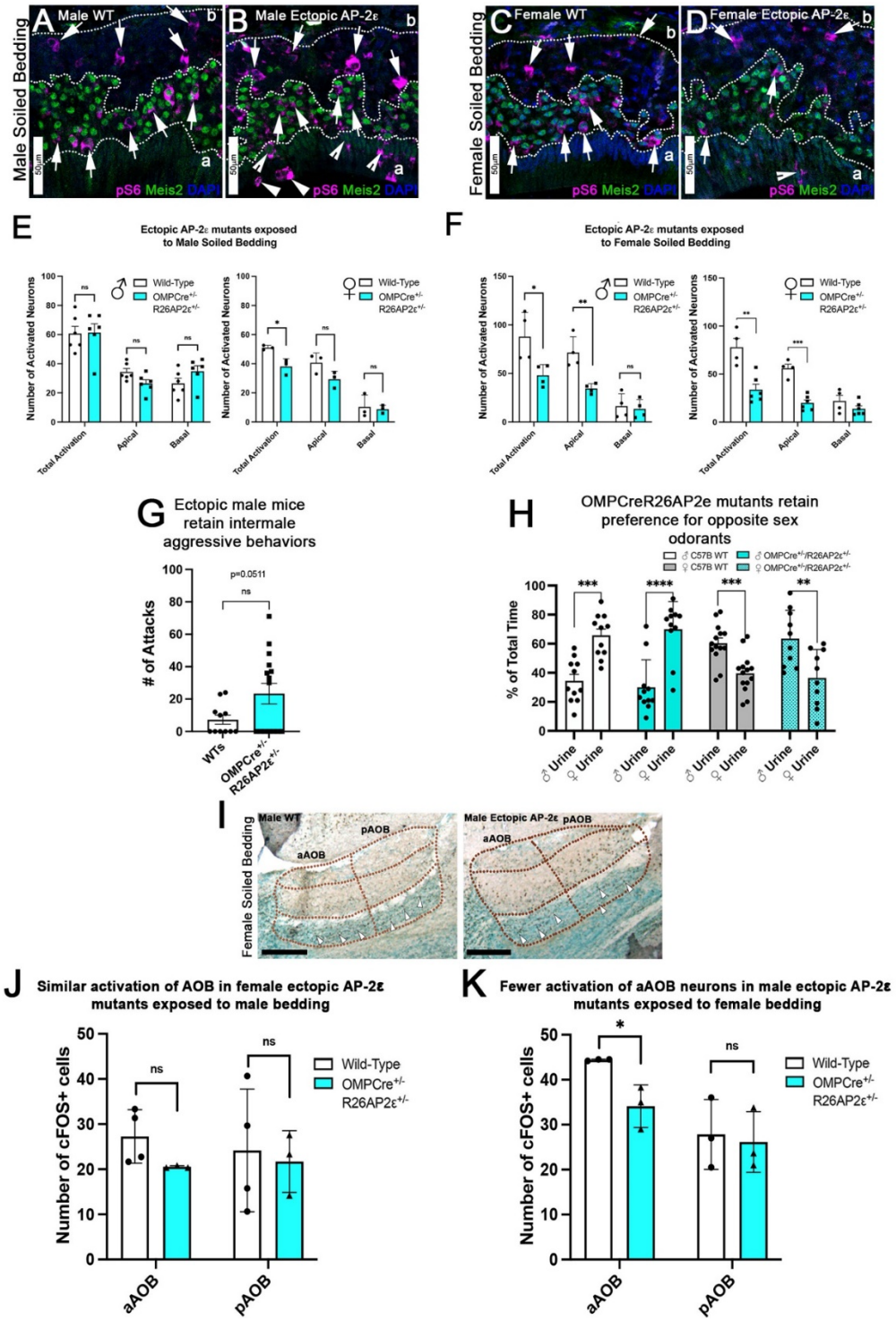

Figure 6: Ectopic AP-2ε expression alters the detection of sex-specific odorants. A-D) Immunofluorescence against pS6 (magenta, arrows) and Meis2 (green) with DAPI counterstain (blue) in the VNE of Controls (A,C) and OMPCreR26AP-2ε mutants (B,D). A,B) VNE of adult male wildtype and ectopic mutants when exposed to male soiled bedding show similar activation or pS6 immunoreactivity (arrows) in Meis2+/apical and Meis2-/basal VSNs. C,D) VNE of adult female wildtype and ectopic mutants when exposed to female soiled bedding show that while WT females displayed a higher proportion of pS6+ apical VSNs, OMPCre$^{+/-}$/R26AP-2ε$^{+/-}$ mutants showed a decreased number of activated Meis2+/apical

VSNs. In both exposure conditions ectopic activation of sustentacular cells (notched arrows) and VSNs near the lumen (arrowheads). E) Quantifications of activated VSNs in male and female mice after exposure to male-soiled bedding show a non-significant decrease in activated apical VSNs in mutants of both sexes. Mutant females show a significant decrease in total activation of VSNs ($p<0.05$) while mutant males show a small but non-significant increase in the total number of activated basal VSNs. N=6 for males and n=3 females for both genotypes F) Quantifications of activated VSNs after exposure to female-soiled bedding in male and female mice show a significant decrease in the number of activated apical VSNs as well as total activation of VSNs between mutants and controls of both sexes ($p<0.05$=*, $p<0.01$=**, $p<0.001$=***). N=4 for males and n=6 for females for both genotypes. G) Quantifications of the number of attacks for all WT and OMPCre$^{+/-}$/R26AP-2$\varepsilon^{+/-}$ mutants in a resident intruder test show male ectopic AP-2ε mice display higher levels of intermale aggression but are not significantly different than controls. N=11 for WTs and n=17 for OMPCre$^{+/-}$/R26AP-2$\varepsilon^{+/-}$ mutants. H) Quantifications of odorant preference tests in male and female mice show that male and female OMPCre$^{+/-}$/R26AP-2$\varepsilon^{+/-}$ mutants retain the preference for opposite sex odorants. ($p<0.05$=*, $p<0.01$=**, $p<0.001$=***, $p<0.0001$=****). N=11 for WT males, n=14 for WT females, n=11 for OMPCre$^{+/-}$/R26AP-2$\varepsilon^{+/-}$ mutant males and n=10 for OMPCre$^{+/-}$/R26AP-2$\varepsilon^{+/-}$ mutant females. I) AOB of adult male wildtype and ectopic mutants when exposed to female soiled bedding show that ectopic mutants have lower levels of cFOS activated neurons in the anterior AOB (aAOB) but similar levels of activated neurons in the posterior AOB (pAOB). Scale bar=250um. J) Quantification of cFOS activated neurons in the AOB of female mice exposed to male-bedding show no significant differences between anterior and posterior AOB activation in mutants and WT. N=4 for WT and n=3 for OMPCre$^{+/-}$/R26AP-2$\varepsilon^{+/-}$ mutants. K) Quantification of cFOS activated neurons in the AOB of male mice exposed to female-soiled bedding show a significant reduction in anterior AOB activation ($p<0.05$) in mutants compared to WT. N=3 for both WT and OMPCre$^{+/-}$/R26AP-2$\varepsilon^{+/-}$ mutants.

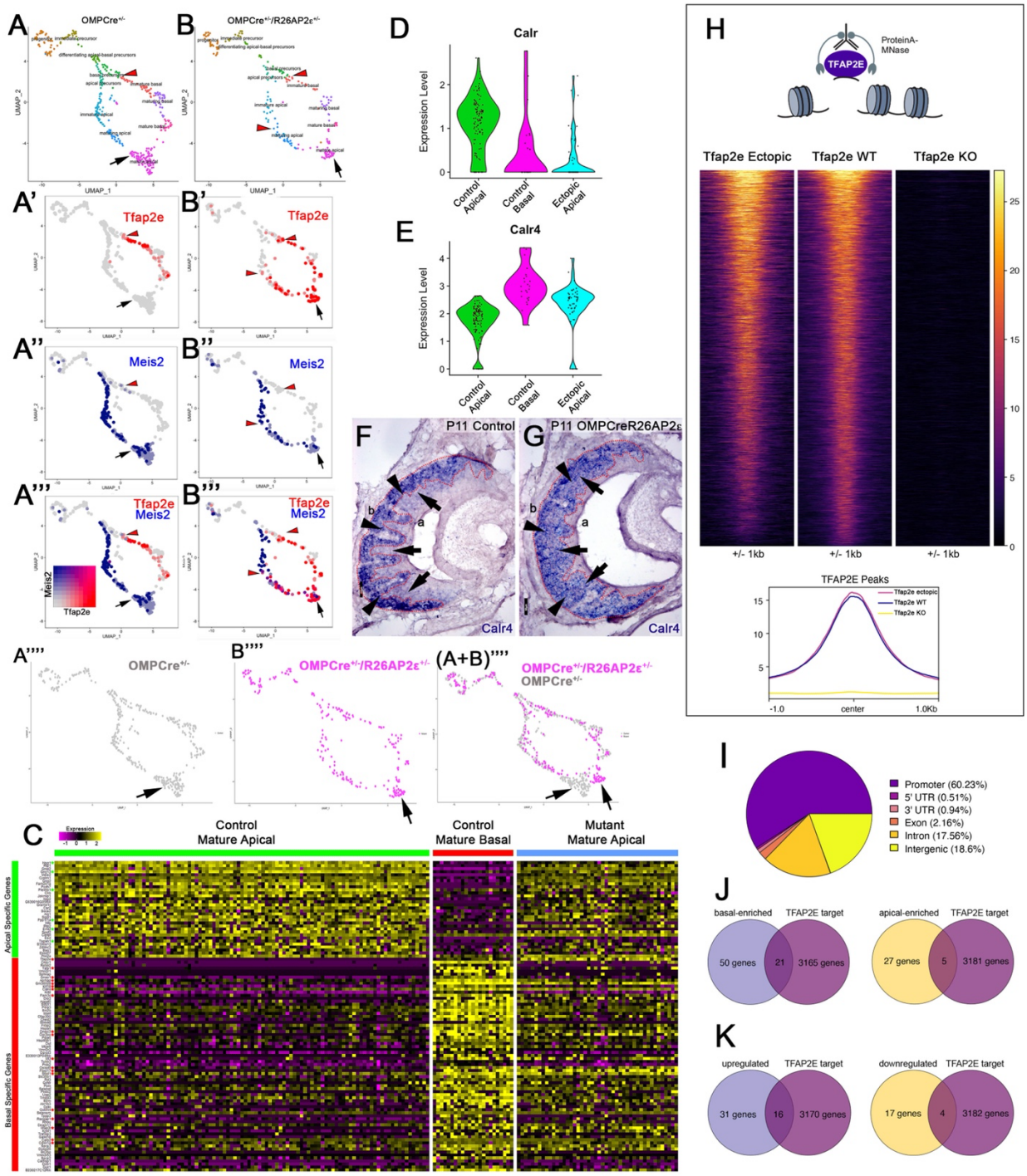

Figure 7: Single-cell sequencing of P10 OMPCre$^{+/-}$ control and OMPCre$^{+/-}$R26AP2ε$^{+/-}$ mutant VSNs indicate a shift in apical cells towards basal cells in the mutant. A-A''') UMAP clustering of VSNs from progenitor cells to differentiated mature apical and basal cells of Control B-B''') Mutant mice split by genotype. A'-A''', B'-B''') Blended feature plots of AP-2ε expression (red) and Meis2 (blue). Red arrowheads indicate onset of AP-2ε expression. Black arrow indicates mature apical VSNs. OMPCre$^{+/-}$ Controls (A'-A''') show a divergent pattern of expression where the onset of AP-2ε (red, red arrowhead) is only on the basal branch. Meis2 expression (blue) occurs only on the apical branch where the cells lack AP-2ε expression. OMPCre$^{+/-}$R26AP2e$^{+/-}$ mutants (B'-B''') start to express AP-2ε on the basal branch in immature basal VSNs (red) however, onset of AP-2ε mRNA expression also occurs on the apical branch (blue). B''') In ectopic

mutants, AP-2ε mRNA is co-expressed with Meis2 in apical VSNs (purple cells). A'''') Feature plot of apical cells in OMPCre$^{+/-}$ controls (black arrow). B'''') Feature plot of apical cells in OMPCre$^{+/-}$R26AP2e$^{+/-}$ mutants (black arrow). (A+B)'''') Overlay shows that apical cells with ectopic AP-2ε expression (magenta, black arrow) clustered separately from mature apical cells of OMPCre$^{+/-}$ controls (gray, black arrow). D) Violin plot shows Calreticulin (Calr) mRNA expression levels in apical VSNs from the OMPCre$^{+/-}$R26AP2ε$^{+/-}$ mutants are reduced to levels similar to basal VSNs from OMPCre$^{+/-}$ controls. E) Violin plot shows Calreticulin-4 (Calr4) mRNA expression levels. E) In control cells, AP-2ε mRNA expression (red arrowheads) and Meis2 mRNA expression (blue) are not co-expressed in the same cells. AP-2ε expression is upregulated in immature basal VSNs and not apical VSNs. F,G) ISH against Calr4 against P11 OMPCre$^{+/-}$ controls (F) and OMPCre$^{+/-}$R26AP2ε$^{+/-}$ mutants (G) show that while Calr4 mRNA is normally enriched in basal VSNs (arrowheads), ectopic AP-2ε mutants show expansion of Calr4 positivity in the apical regions when compared to controls (arrows). H-K) Analysis of CUT&RUN against Tfap2e/AP-2ε. H) Tornado plot of AP-2ε occupancy in Tfap2e ectopic, WT and KOs in the dissociated tissue of the VNO. Tfap2e signal in ectopic mutants and WTs is similar across all Tfap2e peaks, while Tfap2e KOs show no signal. The genomic regions are defined as the summit +/- 1kb. I) Pie chart depicting the genomic distribution of putative AP-2ε binding sites show that most of AP-2ε peaks are found in promoter regions of putative target genes and to a lesser extent in intergenic and intronic regions of the genome. J) Venn diagram of the determined AP-2ε targets and the genes enriched in the basal and apical VSNs. K) Venn diagram of the determined AP-2ε targets and all the upregulated and downregulated genes in the ectopic AP-2ε mutant mouse. Significance defined as Adjusted p-value ≤ 0.05.

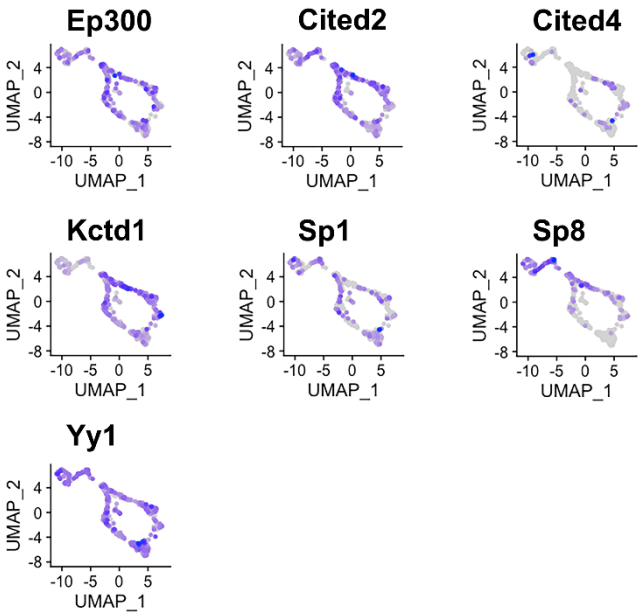

<u>Supplementary Figure S1</u>: Expression of potential AP-2 co-factors in both apical and basal VSNs. Feature plots of known AP-2 family cofactors p300/CBP, Cited2, Cited4, Kctd1, Sp1, Sp8, Yy1 in P10 VSNs.

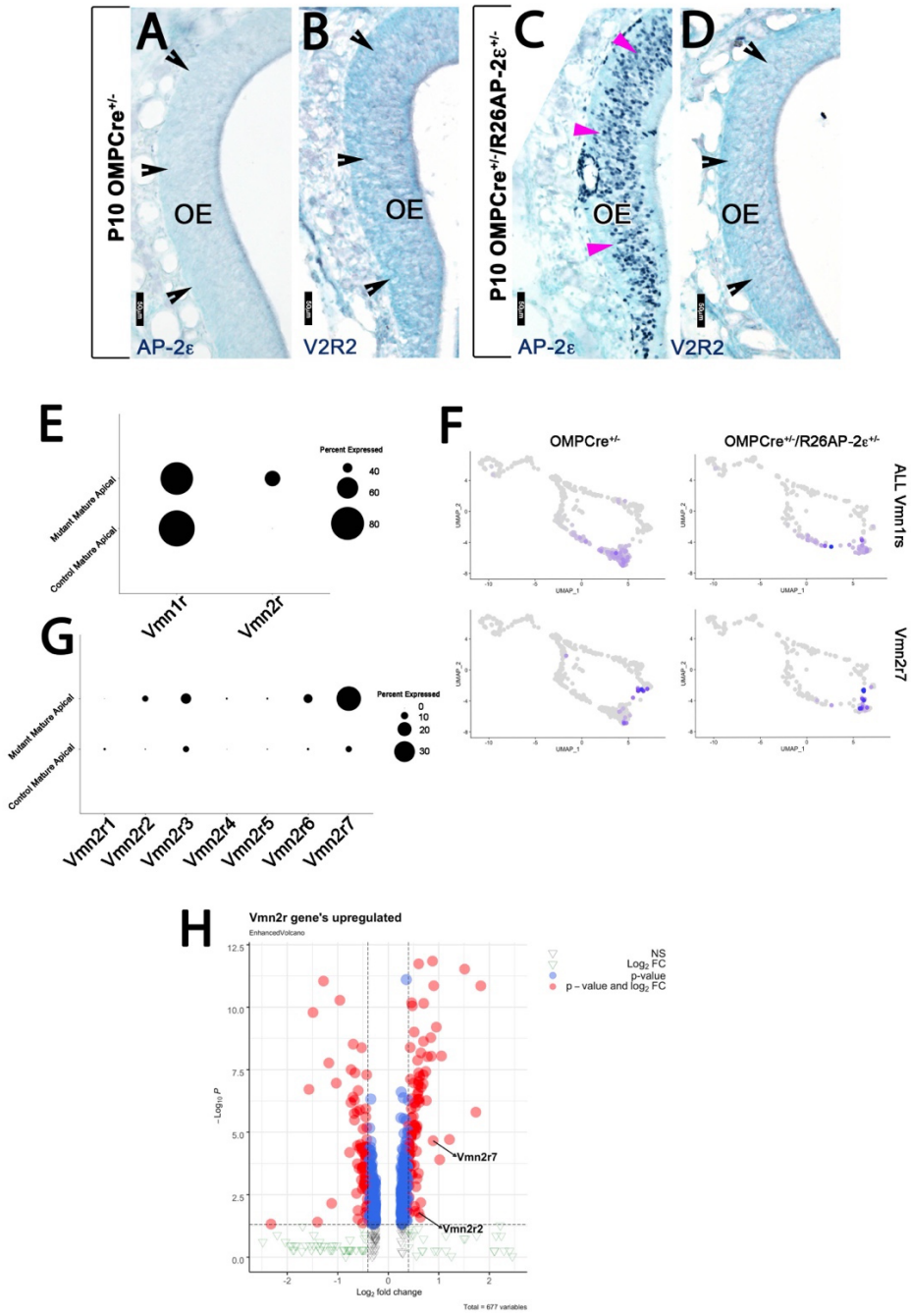

Supplementary Figure S2: **AP-2ε and V2R2 immunoreactivity in the MOE.** P10 OMPCre$^{+/-}$ controls(A,B) and OMPCre$^{+/-}$/R26AP-2ε$^{+/-}$ ectopic mutants (C,D). A,C) Immunohistochemistry against AP-2ε in the main olfactory epithelium (OE) shows no immunoreactivity in controls (black notched arrows) and ectopic AP-2ε expression in the mutants (magenta arrowheads). B,D) Immunohistochemistry against V2R2 in the main olfactory epithelium (OE) shows no expression (black notched arrowheads) in either control nor ectopic AP-2ε mutant.

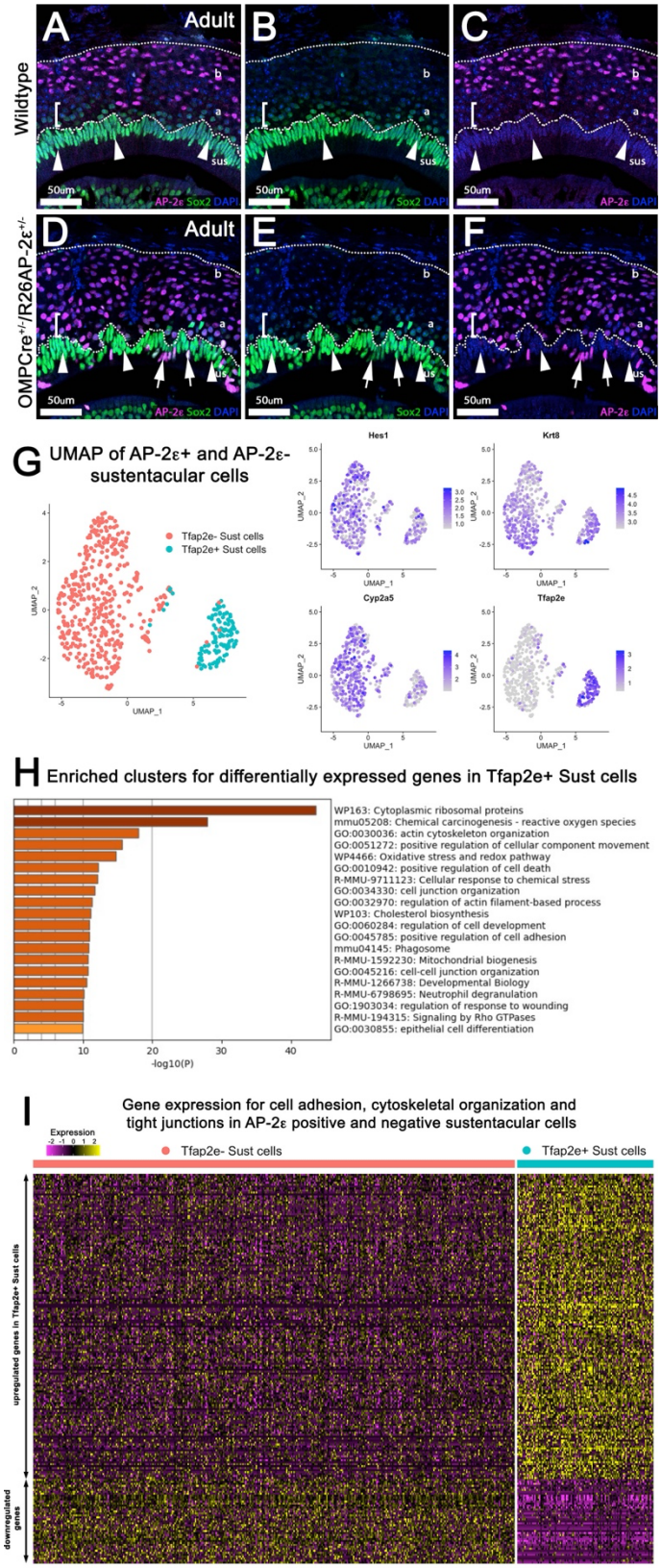

<u>Supplementary Figure S3:</u> Analysis of Sustentacular Cells. A-F) Immunofluorescence on Wildtype (A-C) and OMPCre$^{+/-}$/R26AP2ε$^{+/-}$ mutants (D-F) against AP-2ε (magenta) and Sox2 (green) counterstained with DAPI (blue). A-C) A-C) WT controls and ectopic AP-2ε mutants (D-F) show sustentacular (sus) cells with high immunoreactivity for Sox2 and no AP-2ε expression. Apical (a) VSNs closest to the sustentacular cell layer show low immunoreactivity for Sox2 (brackets, arrowheads) with apical VSNs closer to basal (b) VSNs with no immunodetectable Sox2 (notched arrows). no colocalization between AP-2ε and Sox2+ sustentacular cells (sus). D-F) OMPCre$^{+/-}$/R26AP2ε$^{+/-}$ mice have some Sox2+ sustentacular cells that have ectopic AP-2ε expression (arrows). G) UMAPs of sustentacular cells from OMPCre$^{+/-}$/R26AP2ε$^{+/-}$ adults showed that AP2ε positive and negative clusters segregated from each other with accompanying feature plots showing the expression of sustentacular cell markers Hes1, Krt8, and Cyp2a5 along with ectopic Tfap2e/AP-2ε mRNA expression. H) Gene ontology analysis of Tfap2e+ sustentacular cells showed an enrichment of dysregulated genes related to cytoskeleton organization, cell-cell junction organization, cytoskeletal organization, and cytoplasmic ribosomal proteins. I) Heatmap of up- and down-regulated genes found related to cytoskeleton organization, cell-cell junction organization, and cytoskeleton organization in Tfap2e positive and negative sustentacular cells.

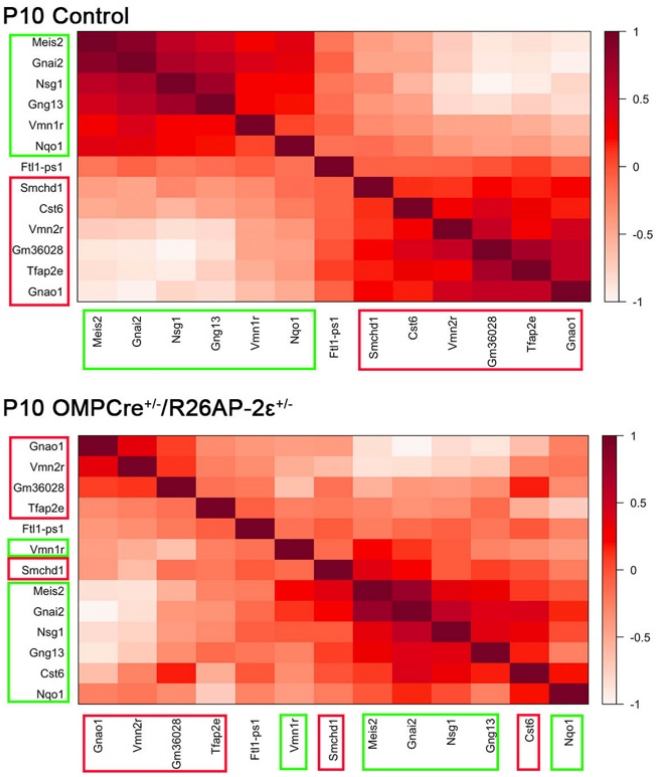

<u>Supplementary Figure</u> S4. Gene Expression Correlation changes after ectopic AP-2ε expression.

In control animals, specific sets of genes are expressed with high correlation level in either apical VSNs (boxed in green) or basal VSNs (boxed in red). Genes with higher expression correlation are close to each other in either X and Y axis, the legend indicates higher correlation of expression with darker shade of red. In OMPCre$^{+/-}$/R26AP2ε$^{+/-}$ mutants, ectopic AP-2ε expression alters the cell type specific genes indicated by the different order of genes and different shades of red/expression correlation. These show that ectopic AP-2ε expression alters the normal correlation of apical and basal enriched genes.

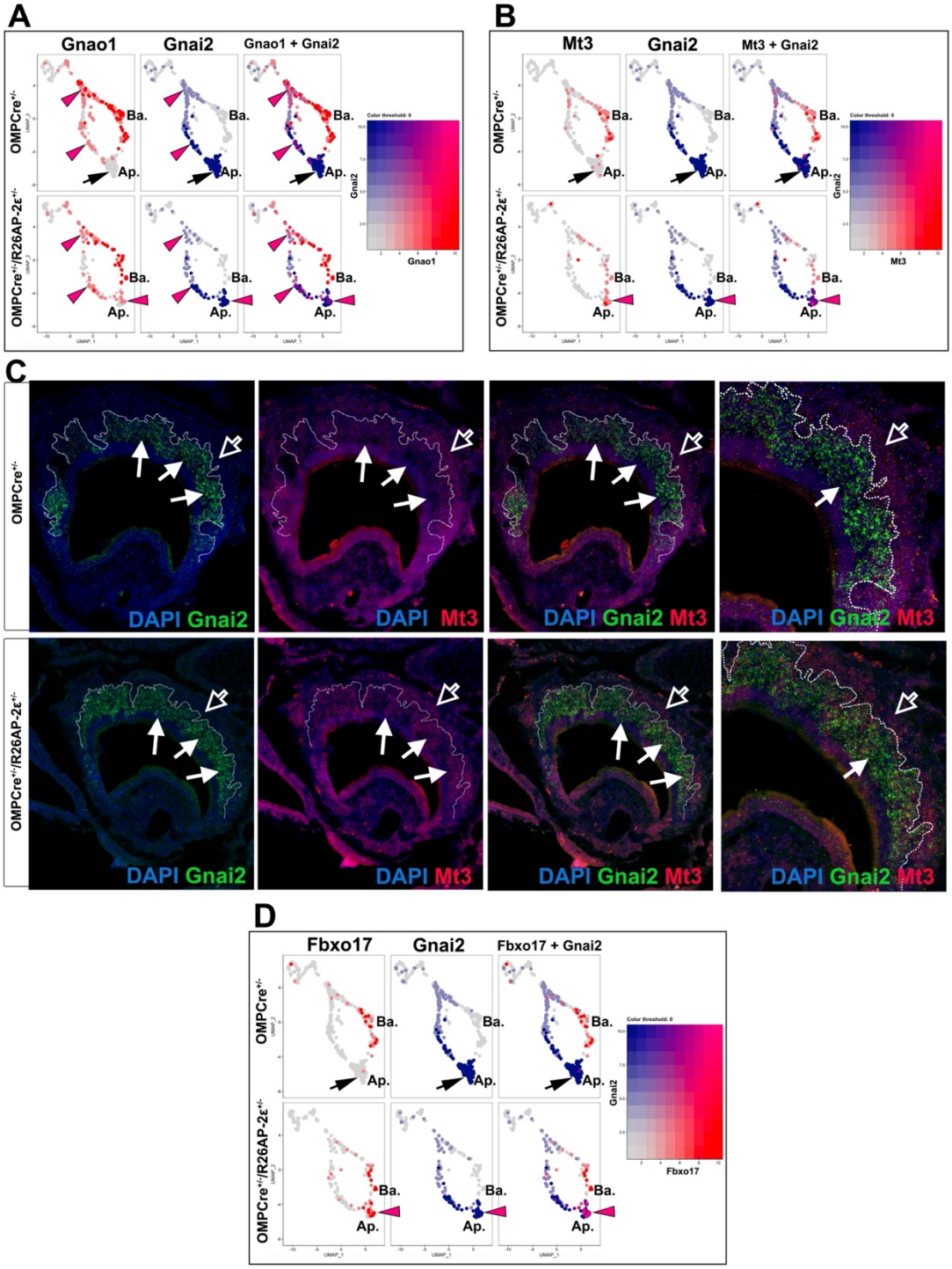

Supplementary Figure S5. Ectopic expression in apical VSNs of indicated genes in OMPCre$^{+/-}$/R26AP-2ε$^{+/-}$ mutants. A) Feature plot showing ectopic expression of Gnao1 in OMPCre$^{+/-}$/R26AP-2ε$^{+/-}$ mutants. Black arrows indicate mature apical VSNs, Purple arrow heads indicate ectopic expression of Gnao1 in apical VSNs. B) Feature plot showing ectopic expression of Mt3 in OMPCre$^{+/-}$/R26AP-2ε$^{+/-}$ mutants. Black arrows indicate mature apical VSNs, Purple arrow heads indicate ectopic expression of Mt3 in

1527 apical VSNs. C) RNAscope analysis shows that Mt3 is mainly expressed in basal VSNs
1528 in OMPCre$^{+/-}$ controls (arrow outline) but ectopically expressed in Gnai2+ apical VSNs in
1529 OMPCre$^{+/-}$/R26AP-2$\varepsilon^{+/-}$ mutants (arrows). D) Feature plot showing ectopic expression of
1530 Fbxo17 in OMPCre$^{+/-}$/R26AP-2$\varepsilon^{+/-}$ mutants. Black arrows indicate mature apical VSNs,
1531 Purple arrow heads indicate ectopic expression of Fbxo17 in apical VS

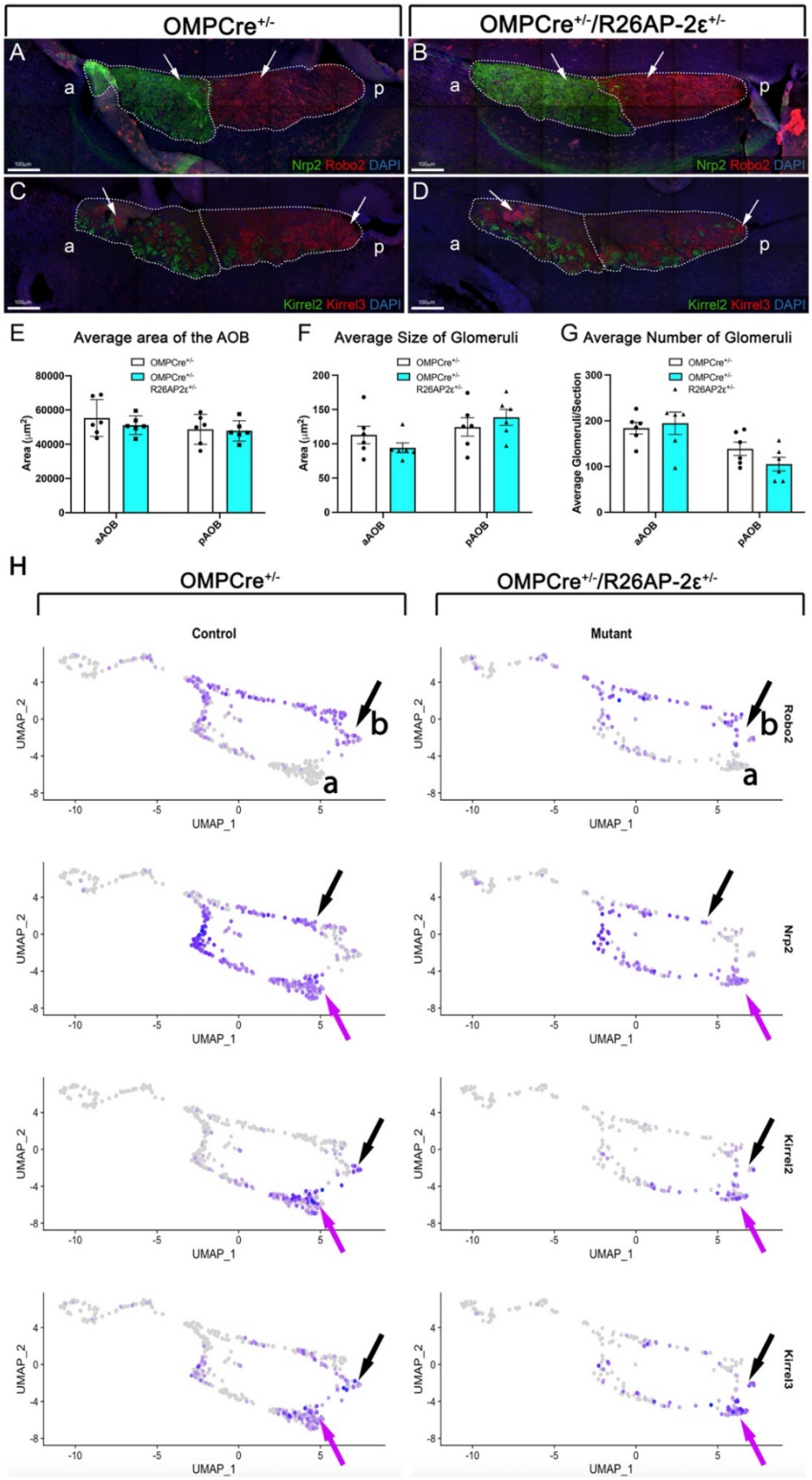

Supplementary Figure S6: Analysis of the AOBs from adult WT and OMPCre$^{+/-}$/R26AP2ε$^{+/-}$ mice. A,B) Immunofluorescence against Nrp2 (green) and Robo2 (red) and counterstained with DAPI (blue) showed that the expression of guidance cue molecules in WT (A) and OMPCre$^{+/-}$/R26AP2ε$^{+/-}$ mutant (B) mice was comparable with distinct anterior and posterior AOB regions (arrows). C,D) Immunofluorescence against Kirrel2 (green) and Kirrel3 (red) and DAPI (blue) counterstain on WT (C) and OMPCre$^{+/-}$/R26AP2ε$^{+/-}$ mutant

mice (D) AOBs showed that the glomerular organization and morphology was comparable between genotypes (arrows). E) Quantifications of the average area of the AOB was not significantly different across genotypes. Analysis of the glomeruli size (F) and number (G) using IF against Kirrel2 and Kirrel3 showed no significant changes across genotypes. N=6 for OMPCre$^{+/-}$ controls and OMPCre$^{+/-}$/R26AP2ε$^{+/-}$ mutants (E-G).

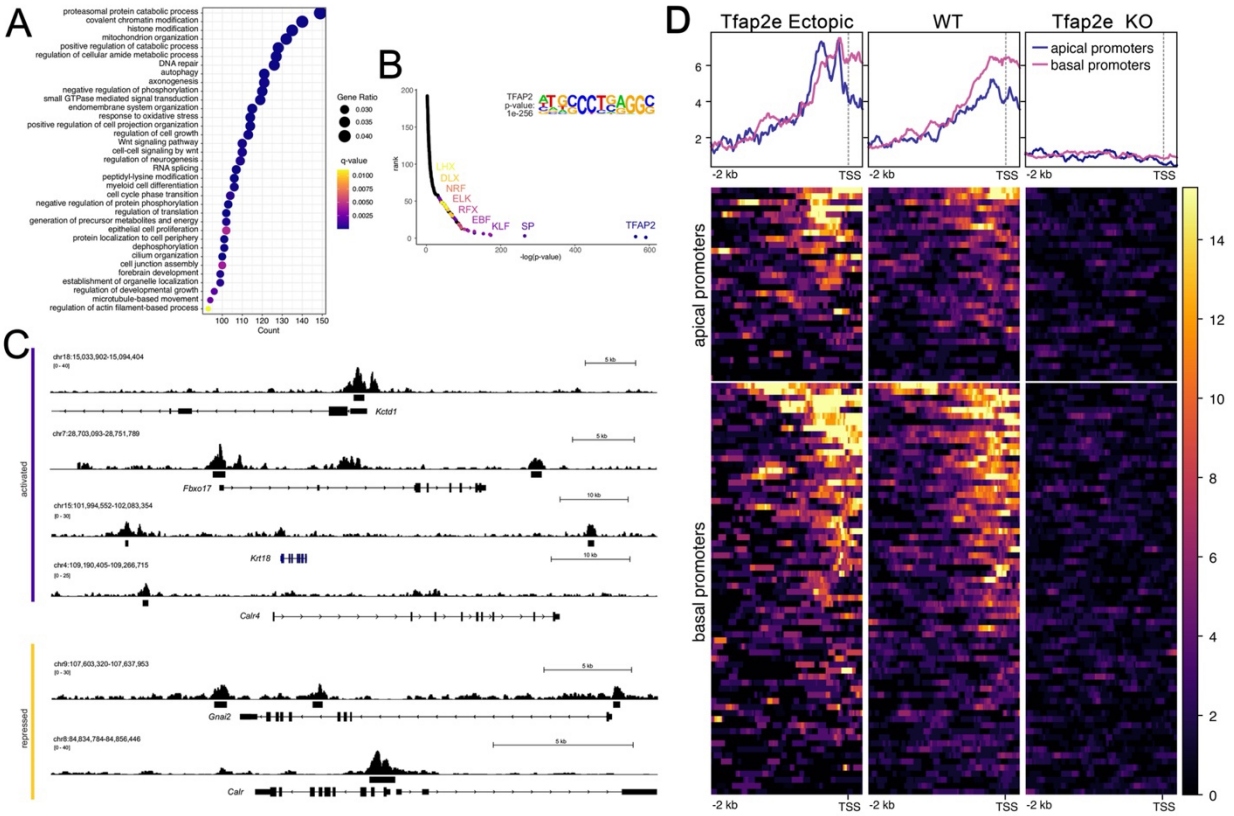

Supplementary Figure S7: A) Dot plot of enriched GO terms show many putative AP-2ε target genes being chromatin or histone modifiers. B) Motif enrichment analysis validated our analysis as Tfap2 was the top motif found at putative binding sites. It also yielded TF family motifs of potential cofactors including SP, KLF, EBF, RFX, ELK, NRF, DLX, and LHX transcription factor families. C) Tracks from CUT&RUN sequencing where AP-2ε peaks are found in the promoter regions of activated (purple) and repressed (yellow) genes. D) Promotor plots of AP-2ε binding in ectopic mutants, WTs and KOs. In WTs, there is more Tfap2e binding at basal promotors compared to apical, however, in ectopic mutants, apical and basal binding is similar due to Tfap2e ectopic expression. Tfap2e KOs show little to no signal.

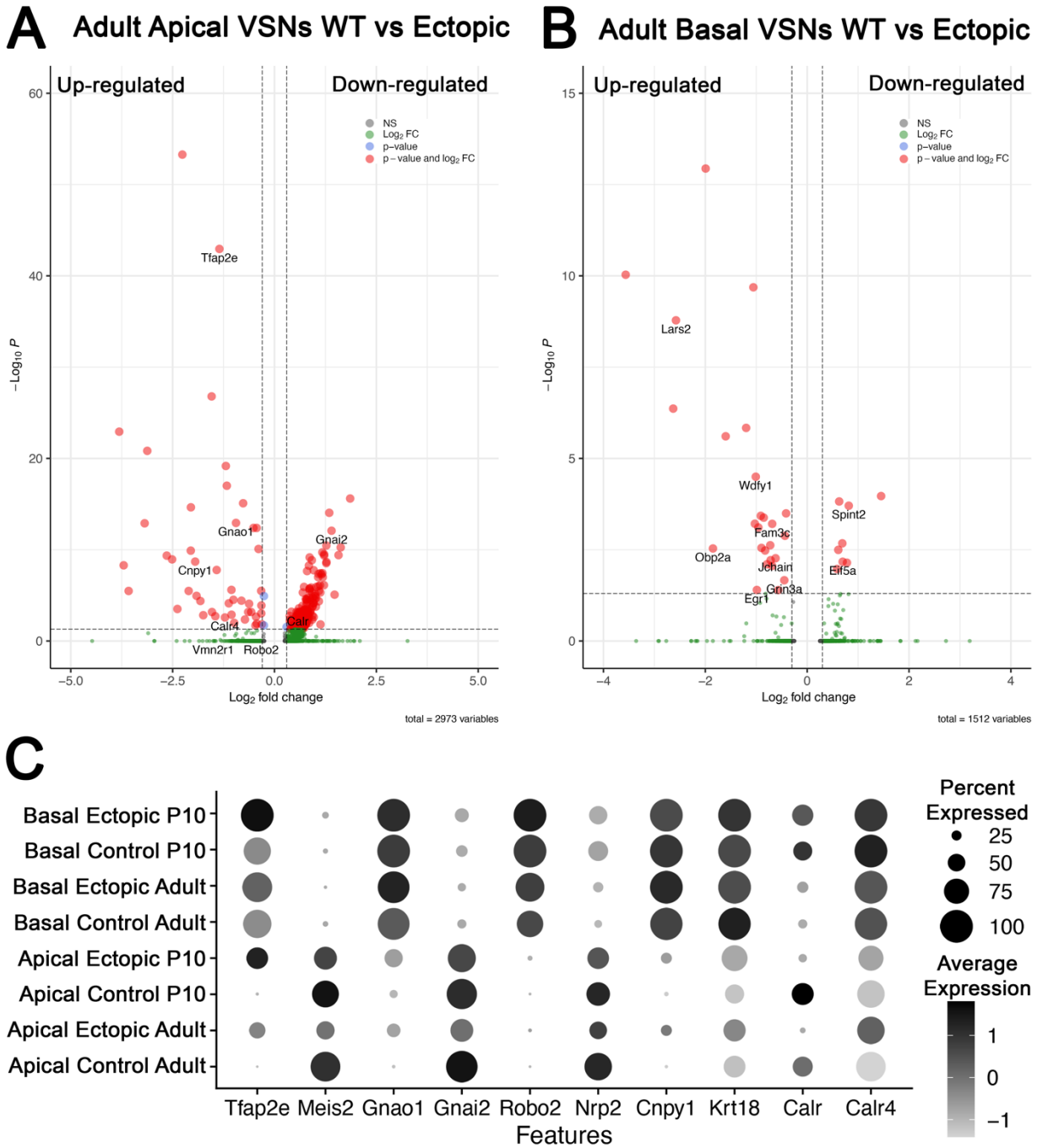

Supplementary Figure S8: Differential gene expression analysis from scSeq in adult animals of apical and basal populations scSeq in Adults WT Controls and OMPCre$^{+/-}$/R26AP2ε$^{+/-}$ VNOs. A) Volcano Plot of significantly up- and down-regulated genes in apical VSNs in adult WT and OMPCre$^{+/-}$/R26AP2ε$^{+/-}$ mice show dysregulation of many key basal genes and down-regulation of apical-enriched genes. B) Volcano Plot of significantly up and downregulated genes in basal VSNs in adult WT and OMPCre$^{+/-}$/R26AP2ε$^{+/-}$ mice show that some genes may respond to AP-2ε regulation in a dose-dependent manner. C) Dot plot of canonical genes expressed by apical and basal VSNs and key genes identified in scSeq analysis for P10 and Adult Control and Mutant mice.

Supplementary Table S1

Differentially expressed genes in mature apical and basal VSNs

Apically Enriched Genes					
Gene Name	P. Value	Average Log Fold Change	Mature Basal %	Mature Apical %	Adjusted P.Value
Nsg1	2.19E-13	-1.9461937	0.87	0.991	4.77E-09
Rtp1	3.99E-13	-1.7210806	0.13	0.972	8.69E-09
Gnai2	1.21E-12	-3.2758293	0.261	0.963	2.63E-08
Gng13	1.44E-12	-2.4998775	0.565	0.981	3.14E-08
Meis2	1.46E-12	-2.3994924	0.087	0.944	3.18E-08
Cystm1	2.60E-12	-1.1223905	0.913	1	5.66E-08
Gng2	4.70E-12	-1.8780287	0.696	0.963	1.02E-07
Fam241a	2.15E-11	-1.3441602	0.304	0.925	4.68E-07
Pcdh7	5.79E-11	-1.1606574	0.043	0.869	1.26E-06
Plekhb1	3.29E-10	-0.8073116	0.739	0.991	7.16E-06
Ckb	5.70E-10	-0.942904	0.957	1	1.24E-05
Jakmip1	2.13E-09	-0.7864416	0.13	0.841	4.65E-05
Nrp2	2.48E-09	-0.9997662	0.565	0.925	5.41E-05
G630016G05Rik	3.62E-09	-0.8518453	0	0.766	7.89E-05
Gramd1c	6.12E-09	-0.8132581	0.304	0.869	1.33E-04
Car2	1.29E-08	-0.871219	0.783	0.963	2.82E-04
Socs2	1.40E-08	-0.8762327	0.913	0.981	3.04E-04
Aig1	1.33E-07	-0.6442775	0.478	0.869	2.91E-03
Sgpl1	1.38E-07	-0.750675	0.652	0.953	3.01E-03
Ppp1r1a	1.62E-07	-0.6387545	0.87	0.953	3.53E-03
Nfix	1.63E-07	-0.6919687	0.087	0.71	3.55E-03
Rtp2	2.67E-07	-0.6124008	0.783	0.925	5.81E-03
Eml2	3.24E-07	-0.4522206	0	0.645	7.05E-03
Spef2	3.76E-07	-0.6257323	0.522	0.907	8.19E-03
Cartpt	6.02E-07	-0.504793	0.957	0.963	1.31E-02
Esd	6.05E-07	-0.5783619	0.174	0.748	1.32E-02
Tspan1	7.99E-07	-0.6642304	0.304	0.785	1.74E-02
S100a13	1.18E-06	-0.6578302	0.217	0.72	2.58E-02
Zdhhc3	1.22E-06	-0.6494611	0.609	0.879	2.65E-02
Bag1	1.60E-06	-0.4936463	0.87	0.972	3.48E-02
Exosc7	1.70E-06	-0.4935659	0.522	0.841	3.71E-02
Prxl2a	1.95E-06	-0.6048927	0.957	1	4.24E-02

Basally Enriched Genes					
Gene Name	P. Value	Average Log Fold Change	Mature Basal %	Mature Apical %	Adjusted P.Value
Tfap2e	2.71E-23	1.01282475	0.87	0.019	5.90E-19
Cnpy1	1.23E-22	2.05509001	1	0.093	2.69E-18
Robo2	3.77E-22	0.90330448	0.957	0.056	8.20E-18
Tafa1	4.72E-21	0.96728089	0.826	0.028	1.03E-16
Vmn2r1	2.11E-19	1.2793116	0.783	0.028	4.59E-15
Sphkap	6.49E-15	0.28031925	0.522	0	1.41E-10
Gnao1	6.12E-14	1.42314493	0.957	0.327	1.33E-09
Apmap	1.17E-13	1.58179511	1	0.916	2.55E-09
Gm36028	1.19E-13	2.53665489	1	0.682	2.58E-09
Krt18	2.60E-13	1.6051759	1	0.673	5.67E-09
Calr4	6.57E-13	1.39565197	1	0.916	1.43E-08
Krt8	1.51E-12	1.68676872	0.957	0.551	3.28E-08
Fam3c	1.65E-12	1.07729387	1	0.664	3.60E-08
Dio3	1.68E-12	0.40528977	0.478	0.009	3.65E-08
Agpat5	1.79E-12	1.08439932	1	0.514	3.89E-08
Sdf2l1	5.07E-12	1.50705224	1	0.879	1.10E-07
Pdia3	6.16E-12	0.86129121	1	1	1.34E-07
Itm2b	7.96E-12	1.18425959	1	1	1.73E-07
Manf	1.07E-11	1.37611844	1	0.953	2.33E-07
Cfap300	2.16E-11	0.77700954	0.957	0.421	4.71E-07
Creld2	2.17E-11	1.00229149	0.957	0.523	4.73E-07
Shisa8	2.58E-11	0.36615576	0.391	0	5.63E-07
Fkbp2	2.90E-11	0.72341813	1	0.907	6.32E-07
Hspa5	5.22E-11	1.40010137	1	0.981	1.14E-06
Dnajc3	6.37E-11	1.1592286	0.957	0.729	1.39E-06
Dio3os	7.37E-11	0.49488572	0.565	0.047	1.60E-06
Pdia6	1.07E-10	1.14235131	1	0.888	2.32E-06
Hsp90b1	2.05E-10	0.85553036	1	0.991	4.47E-06
Dut	2.84E-10	0.76430257	1	0.86	6.19E-06
Mfge8	3.07E-10	1.07748862	0.957	0.794	6.68E-06
Vmn2r2	4.22E-10	1.35916407	0.391	0.009	9.19E-06
Dpysl3	1.30E-09	1.17193306	0.957	0.757	2.84E-05
E330013P04Rik	1.41E-09	0.35778211	0.609	0.084	3.08E-05
Mt3	1.88E-09	0.57279227	0.739	0.215	4.09E-05
Tubb3	3.51E-09	0.64687805	1	0.963	7.64E-05
Prdx2	3.78E-09	0.72277812	1	0.953	8.23E-05
Osbpl9	5.01E-09	0.83250073	0.913	0.813	1.09E-04

Fbxo17	5.56E-09	0.50343797	0.652	0.15	1.21E-04
Stbd1	6.55E-09	1.09297275	1	0.963	1.43E-04
Slc35b1	9.68E-09	0.68626655	0.957	0.738	2.11E-04
Rd3	1.35E-08	0.5858953	1	0.972	2.93E-04
Gchfr	1.35E-08	0.32772543	0.522	0.065	2.94E-04
Ppib	1.55E-08	0.6188014	1	0.972	3.38E-04
Selenof	1.55E-08	0.51120029	1	0.981	3.38E-04
Plxdc2	1.59E-08	0.2695123	0.435	0.037	3.45E-04
Ugp2	1.63E-08	0.90939627	0.957	0.794	3.56E-04
Tmed3	2.62E-08	0.50570554	1	0.916	5.71E-04
B2m	3.78E-08	1.26181829	0.913	0.542	8.23E-04
Akr1b3	6.06E-08	0.97983293	0.87	0.523	1.32E-03
Optn	7.24E-08	0.31830823	0.478	0.065	1.58E-03
Golim4	8.68E-08	0.52488666	0.913	0.551	1.89E-03
Selenom	1.04E-07	0.49334844	1	1	2.26E-03
Tppp3	1.17E-07	0.89025439	0.652	0.168	2.55E-03
Racgap1	1.58E-07	0.61403494	0.913	0.561	3.45E-03
Rhou	1.72E-07	0.39239137	0.609	0.15	3.74E-03
Dnajb11	1.76E-07	0.70097289	0.957	0.944	3.84E-03
Mfap3l	2.28E-07	0.28167932	0.565	0.103	4.96E-03
Kctd1	2.38E-07	0.88812556	0.913	0.542	5.17E-03
Traf3ip3	3.03E-07	0.73231367	0.391	0.037	6.61E-03
Galnt18	3.24E-07	0.55665364	0.826	0.411	7.05E-03
Calb2	3.73E-07	0.43308595	1	1	8.13E-03
Cdkn1a	3.82E-07	0.5373044	0.957	0.907	8.33E-03
Spcs3	4.63E-07	0.55754661	0.957	0.832	1.01E-02
Dusp26	4.98E-07	0.54873277	0.957	0.822	1.08E-02
Bri3bp	6.03E-07	0.36483009	0.522	0.112	1.31E-02
Vmn2r53	1.01E-06	2.68138046	0.217	0	2.21E-02
Spcs2	1.09E-06	0.59703272	0.957	0.944	2.37E-02
Carhsp1	1.32E-06	0.38531423	0.522	0.112	2.87E-02
Dclk1	2.00E-06	0.39895571	0.826	0.327	4.35E-02
Guk1	2.05E-06	0.5985497	0.913	0.897	4.45E-02
B230217C12Rik	2.24E-06	0.424191	1	0.813	4.87E-02

Supplementary Table S2

Significantly dysregulated genes when Tfap2e/AP-2ε is ectopically expressed in apical VSNs

Significantly Down-Regulated Genes

Gene Name	P. Value	Average Log Fold Change	Mature OMPCre$^{+/-}$ /R26AP2ε$^{+/-}$ Apical %	Mature OMPCre$^{+/-}$ Apical %	Adjusted P.Value
Nsg1	1.05E-19	-1.026049429	0.978	0.991	2.28E-15
Ckb	3.16E-13	-0.832807392	0.957	1	6.89E-09
Plekhb1	1.02E-12	-0.66365877	0.804	0.991	2.23E-08
Calr	1.99E-12	-0.848017913	0.326	0.879	4.33E-08
Gng13	3.92E-11	-0.851799068	0.978	0.981	8.55E-07
Prdx1	6.92E-11	-0.670948424	0.674	0.925	1.51E-06
Ftl1-ps1	5.23E-10	-1.01755918	0.5	0.822	1.14E-05
Calm2	7.50E-09	-0.359436172	1	1	1.63E-04
Rps4x	9.27E-09	-0.462870937	0.978	1	2.02E-04
Chgb	5.21E-08	-0.509353353	0.63	0.907	1.13E-03
Obp2a	5.51E-08	-0.803452485	0.5	0.832	1.20E-03
Esd	1.16E-07	-0.447142323	0.391	0.748	2.54E-03
Eml2	1.21E-07	-0.290177152	0.152	0.645	2.63E-03
Lcn3	3.31E-07	-0.704072872	0.413	0.804	7.22E-03
Nqo1	4.44E-07	-1.080448365	0.239	0.636	9.68E-03
Ppp1r1a	6.98E-07	-0.395511356	0.935	0.953	1.52E-02
Id4	9.43E-07	-0.48810942	0.283	0.673	2.05E-02
Tspan1	1.12E-06	-0.469458509	0.543	0.785	2.45E-02
Cpe	1.20E-06	-0.310695303	1	1	2.61E-02
Gt(ROSA)26Sor	1.32E-06	-0.45231242	0.717	0.832	2.88E-02
Tstd1	1.35E-06	-0.387425488	0.935	0.963	2.94E-02

Significantly Up-Regulated Genes					
Gene Name	P. Value	Average Log Fold Change	Mature OMPCre$^{+/-}$ /R26AP2ε$^{+/-}$ Apical %	Mature OMPCre$^{+/-}$ Apical %	Adjusted P.Value
Abca7	2.79E-10	0.467733988	0.848	0.393	6.07E-06
Apmap	4.12E-08	0.499754357	1	0.916	0.000898417
Calb2	2.04E-08	0.32207374	1	1	0.00044526
Calr4	6.89E-11	0.580533012	0.935	0.916	1.50177E-06
Ccdc136	1.17E-08	0.433981247	0.696	0.252	0.000254306
Cdkn1a	2.88E-07	0.455507857	1	0.907	0.006262153
Cst6	3.50E-14	1.099290617	0.935	0.794	7.62225E-10
Dbi	3.62E-12	1.062519896	0.957	0.813	7.8747E-08
Dio3os	1.34E-15	0.383916442	0.652	0.047	2.92422E-11
Dlx4	8.01E-09	0.438918572	0.783	0.327	0.000174394

Dnajc3	5.15E-07	0.423663136	0.913	0.729	0.011213757
Dusp15	1.60E-08	0.288331862	0.587	0.14	0.00034899
Dync1i1	3.35E-08	0.495088228	0.848	0.533	0.000729768
Enpp1	1.92E-06	0.36206672	0.891	0.551	0.041912856
Fam3c	3.92E-07	0.381794339	0.913	0.664	0.008538247
Fbxo17	1.06E-17	0.668034836	0.804	0.15	2.31481E-13
Fmnl2	1.47E-06	0.294102212	0.717	0.346	0.031962548
Gm36028	1.51E-15	1.565013376	0.935	0.682	3.27889E-11
Gnao1	5.65E-07	0.344705173	0.783	0.327	0.012315414
Golim4	1.06E-06	0.393270819	0.804	0.551	0.023038974
Itpr1	1.54E-12	0.42801754	0.696	0.131	3.35489E-08
Jak1	1.57E-07	0.423690646	0.978	0.972	0.003418952
Kctd1	7.64E-16	0.85428255	0.978	0.542	1.66452E-11
Kctd17	5.75E-08	0.383015359	0.957	0.907	0.001251818
Khdrbs1	9.29E-07	0.388803088	0.935	0.692	0.020230178
Krt18	2.14E-06	0.448568282	0.935	0.673	0.046678066
Lrrc58	5.13E-09	0.336180339	0.717	0.243	0.00011176
Mab21l2	3.38E-11	0.342240813	0.37	0	7.3587E-07
Mapk8ip2	1.52E-07	0.38275929	1	0.963	0.003310007
Mfap3l	5.77E-11	0.330339336	0.609	0.103	1.25577E-06
Mfge8	7.50E-08	0.517438515	0.913	0.794	0.001634157
Mgat5	3.40E-07	0.328523537	0.87	0.486	0.007398101
Mt3	2.31E-12	0.486337274	0.761	0.215	5.03186E-08
Osbpl9	3.00E-09	0.615805448	0.957	0.813	6.544E-05
Pir	6.37E-09	0.572417884	0.848	0.486	0.000138796
Ptprd	4.71E-07	0.333394508	0.522	0.14	0.010266165
Racgap1	1.11E-06	0.405891754	0.87	0.561	0.024189968
Rims3	2.59E-07	0.430808566	1	0.916	0.005638623
Rmdn3	2.84E-08	0.443857099	0.783	0.458	0.000618452
Rpl11	2.14E-07	0.287691748	0.978	0.981	0.004668027
Smchd1	6.17E-13	1.30491047	0.935	0.598	1.34339E-08
Spats2	3.38E-12	0.613696552	0.957	0.832	7.36795E-08
Stbd1	1.62E-08	0.724116114	0.978	0.963	0.000353362
Suox	9.51E-08	0.433632116	0.739	0.364	0.002071784
Tafa1	1.26E-13	0.39251169	0.522	0.028	2.74227E-09
Tfap2e	7.33E-30	2.020231614	0.935	0.019	1.597E-25
Tsnax	2.00E-08	0.574771495	1	1	0.000435139